AFRL-AFOSR-UK-TR-2015-0040

Mechanisms of residual stress generation in mechanical surface treatment: the role of cyclic plasticity and texture

S. Zabeen
M. K. Khan
M. E. Fitzpatrick

THE OPEN UNIVERSITY
WALTON HALL
MILTON KEYNES MK7 6AA UNITED KINGDOM

EOARD Grant #FA8655-12-1-2084

Report Date: August 2015

Final Report from 1 June 2012 to 31 May 2015

Air Force Research Laboratory
Air Force Office of Scientific Research
European Office of Aerospace Research and Development
Unit 4515, APO AE 09421-4515

REPORT DOCUMENTATION PAGE

Form Approved OMB No. 0704-0188

1. REPORT DATE *(DD-MM-YYYY)*	2. REPORT TYPE	3. DATES COVERED *(From – To)*
24 August 2015	Final Report	1 June 2012 – 31 May 2015

4. TITLE AND SUBTITLE

Mechanisms of residual stress generation in mechanical surface treatment: the role of cyclic plasticity and texture

5a. CONTRACT NUMBER

5b. GRANT NUMBER

FA8655-12-1-2084

5c. PROGRAM ELEMENT NUMBER

61102F

6. AUTHOR(S)

S. Zabeen
M. K. Khan
M. E. Fitzpatrick

5d. PROJECT NUMBER

5d. TASK NUMBER

5e. WORK UNIT NUMBER

7. PERFORMING ORGANIZATION NAME(S) AND ADDRESS(ES)
THE OPEN UNIVERSITY
WALTON HALL
MILTON KEYNES MK7 6AA UNITED KINGDOM

8. PERFORMING ORGANIZATION REPORT NUMBER

N/A

9. SPONSORING/MONITORING AGENCY NAME(S) AND ADDRESS(ES)

EOARD
Unit 4515
APO AE 09421-4515

10. SPONSOR/MONITOR'S ACRONYM(S)

AFRL/AFOSR/IOE (EOARD)

11. SPONSOR/MONITOR'S REPORT NUMBER(S)

AFRL-AFOSR-UK-TR-2015-0040

12. DISTRIBUTION/AVAILABILITY STATEMENT

Distribution A: Approved for public release; distribution is unlimited.

13. SUPPLEMENTARY NOTES

14. ABSTRACT

This project investigated the response of two aluminum alloys to laser shock peening, studying the effects of hardening response through different heat treatments of the same alloy; and the effects of crystallographic texture. The hardness of the material after peening was characterized by the nanoindentation technique, and the residual stresses were characterized by the incremental hole drilling technique. The effect of laser peening parameters on the magnitude, depth, and the uniformity of the induced hardness and residual stress was investigated. The number of peen layers has a significant effect on the hardness as well as the residual stress response. The T351 material showed an increase in hardness for up to 4 layers of peening which then saturated with further increase of power density and number of layers. However, an apparent softening effect was observed for the T39 alloy at higher energies. The effect of texture on the residual stresses generated by LSP was also studied. An AlG2099 (an AlGLi alloy) extruded TGbar was used that has strong fibre texture in the web section and a weak rolling texture in the flange section. Results show evidence of the influence of preferred crystallographic orientation on the depth and magnitude of the induced residual stress.

15. SUBJECT TERMS

EOARD, LSP, residual stress, structural components

16. SECURITY CLASSIFICATION OF:			17. LIMITATION OF ABSTRACT	18, NUMBER OF PAGES	19a. NAME OF RESPONSIBLE PERSON
a. REPORT	b. ABSTRACT	c. THIS PAGE			Matt Snyder
UNCLAS	UNCLAS	UNCLAS	SAR	49	19b. TELEPHONE NUMBER *(Include area code)* +44 (0)1895 616420

Mechanisms of residual stress generation in mechanical surface treatment: the role of cyclic plasticity and texture

S. Zabeen, M. K. Khan, M. E. Fitzpatrick

Faculty of Engineering and Computing, Coventry University, Priory Street, Coventry CV1 5FB, UK

AFRL Technical Lead: K. Langer

Final report to the European Office of Research and Development, in fulfilment of grant FA8655-12-1-2084.

LIMITATION OF LIABILITY – Whilst Coventry University believes that the information given in this document is correct at the date of publication it does not guarantee that this is so, nor that the information is suitable for any particular purpose. Users must therefore satisfy themselves as to the suitability of the information for the purpose for which they require it and must make all checks they deem necessary to verify the accuracy thereof. Coventry University shall not be liable for any loss or damage (except for death or personal injury caused by negligence) arising from any use to which the information is put.

Abstract

This project investigated the response of two aluminium alloys to laser shock peening, studying the effects of hardening response through different heat treatments of the same alloy; and the effects of crystallographic texture.

Al-2624 was studied in two heat treatment conditions, T351 and T39, that have different yield strengths and hardening capacity: hence the effect of multiple peen layers on a material that has nominally identical physical properties but with different yield stress and hardening response has been studied. The hardness of the material after peening was characterised by the nanoindentation technique, and the residual stresses were characterised by the incremental hole drilling technique.

The effect of laser peening parameters – specifically laser power density, number of peen layers, spot size, and laser pulse duration – on the magnitude, depth, and the uniformity of the induced hardness and residual stress was investigated. The number of peen layers has a significant effect on the hardness as well as the residual stress response. The T351 material showed an increase in hardness for up to 4 layers of peening which then saturated with further increase of power density and number of layers. However, an apparent softening effect was observed for the T39 alloy at higher energies.

The effect of texture on the residual stresses generated by LSP was also studied. An Al-2099 (an Al-Li alloy) extruded T-bar was used that has strong <111> fibre texture in the web section and a weak rolling texture in the flange section. Results show evidence of the influence of preferred crystallographic orientation on the depth and magnitude of the induced residual stress.

Chapter 1. Introduction

Laser shock peening (LSP) is an emerging technology that offers life extension of engineering components (Sticchi et al. 2014, Hatamleh, Lyons & Forman 2007, King et al. 2006, Hill, Pistochini & and Dewald 2005, Nikitin et al. 2004, Altenberger et al. 2002, Montross et al. 2002, Ruschau et al. 1999, Hong, and Chengye 1998, Zhang et al. 1997, Clauer 1996, Clauer, Walters & and Ford 1983). The fatigue life improvement from LSP is largely dependent on the residual stress distribution generated by the LSP process, which in turn relies upon the choice of the peening parameters. Application of LSP requires extensive characterization of the residual stress distribution induced by peening at different combinations of peening conditions. Whilst the beneficial effect of LSP in improving the fatigue life is well recognized, the mechanistic principles are yet to be fully established. Currently, the structural design process is based on trial-and-error without a detailed understanding of the correlation between the plastic deformation and the consequent hardening and generation of residual stress. At present, therefore, developing an LSP-based fatigue design for enhanced structural integrity is costly and time-consuming. The current research will aid the application of the technology by quantifying the relationships between peening conditions, induced residual stresses and hardness, and material state; and also by providing validation data for various predictive models that will apply these relationships to complex structural geometries.

A systematic study on the effect of single vs. multiple peen overlaps at different peening intensity, and with different peen spot patterning (with respect to the possible crack growth direction) is still lacking. Previously we have applied synchrotron X-ray diffraction to measure the residual stress along a single peened line in Al-2024 alloy (Dorman et al. 2012). The results showed an asymmetric stress profile with a markedly tensile stress region at the centre of the peen spot, which is of great concern from the fatigue-life point of view. To ensure the maximum life benefit from the peening process a fundamental understanding of how peening induces hardening and residual stress is crucial. This can be achieved by modelling, which is being undertaken within the Air Force Research Laboratory at Wright-Patterson AFB. To validate the model experimental residual stress results at different peening conditions are required.

This report presents the effect of peening energy and the number of layers on the hardness and residual stress in Al 2624 alloy in T351 and T39 heat treatment conditions. The cyclic stress-strain behaviour of the material was also examined to understand the hardening response as a function of laser power density and number of layers. The effect of texture on the residual stresses generated by LSP is also investigated.

Chapter 2. Materials and Experimental Method

2.1 Materials

Al-2624 alloy was used in two heat treatment conditions (T351 & T39) for this investigation. T351 comprises solution heat treatment, stress-relief by stretching, and natural aging; whereas T39 is cold worked and naturally-aged after solution heat treatment. The materials were received as plates with a thickness of 25 mm. The microstructure for T351 and T39 alloy is shown in Figure 2-2a and b respectively. The test coupons for residual stress measurement are 70 × 70 mm^2 (see Figure 2-1a) with thickness of 12.7 mm. The specimens were extracted from Al-2624 plates using a wire electro-discharge machine (EDM). Since a smooth surface finish was required in order to get a smooth surface for peening, a surface finish of R_a = 1 was achieved by EDM skim cut settings. A total of 24 specimens were prepared, 12 from each alloy.

Peening was carried out by Metal Improvement Company, at Earby, UK; and by LSP Technologies, Columbus, OH, USA. The peening parameters are given in Tables 2 and 3 respectively. The peening is shown in Figure 2-1b for the single shot configuration. The microstructure for Al-2624 T351 and T39 alloy is given in Figure 2-2 a and b respectively.

Al-2099 alloy was used to study the effect of texture on the residual stress generation owing to LSP. Material was received in the form of an extruded T-bar from Alcoa Inc. Two types of specimens were extracted with dimensions 50 × 50 × 20 mm^3 from the extruded bar (see Figure 2-9) from the web and flange sections to study the texture variation in the material. Once the texture measurement was completed, 12 further specimens were extracted from the web and flange sections. The specimens were extracted in XY, YZ and ZX orientations.

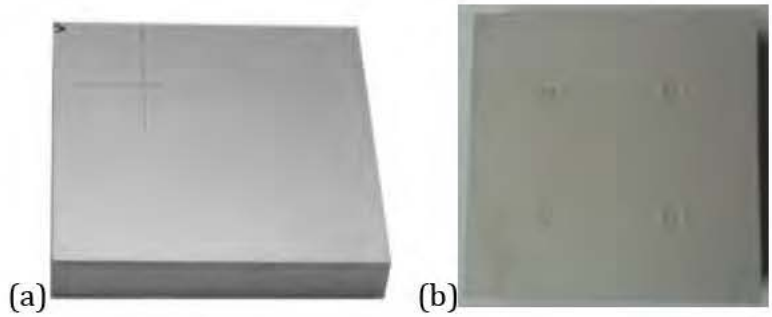

Figure 2-1: Test coupon for residual stress measurement

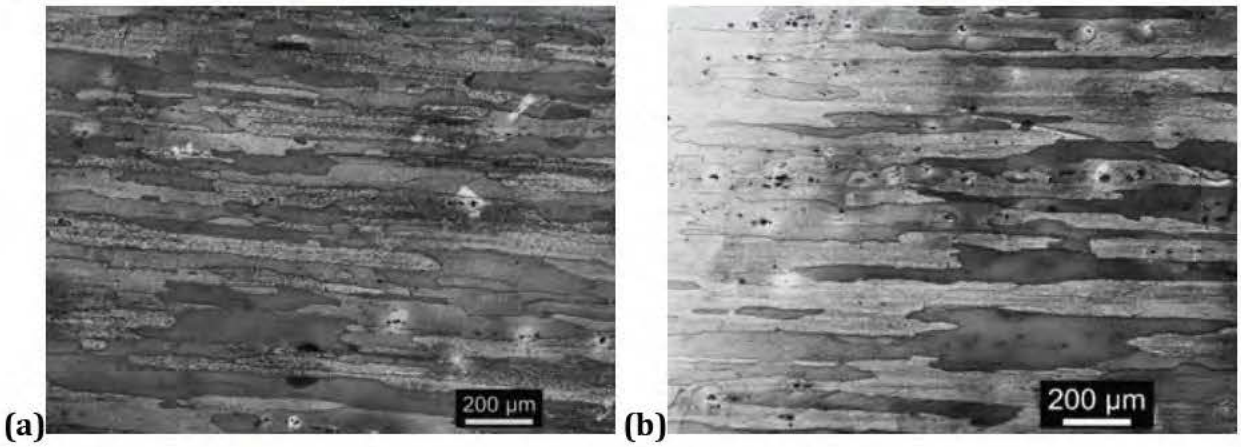

Figure 2-2: Microstructure of Al-2624 alloy, (a) for T351 and (b) T-39 heat treatment condition.

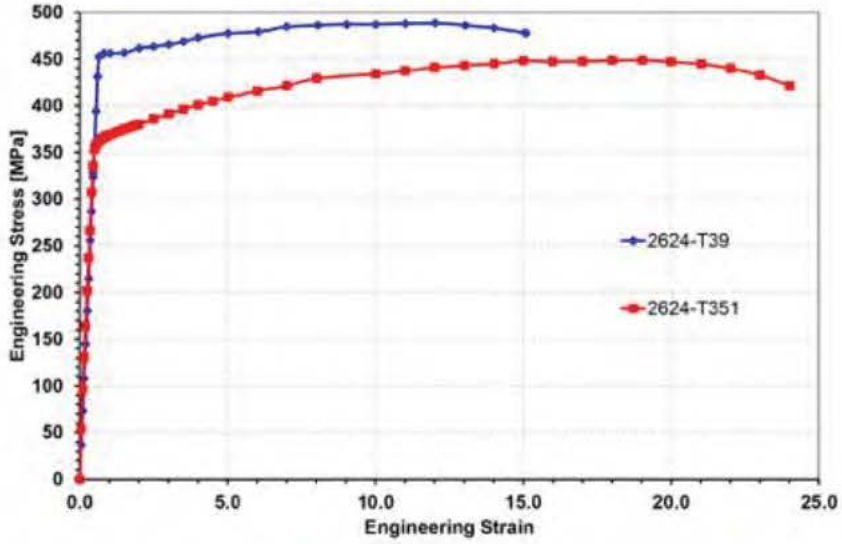

Figure 2-3: Stress–strain curve for Al-2624 alloy in T351 and T39 conditions (Heiniman 2013)

Heat Treatment	Elastic Modulus / GPa	Yield Strength σ_y / MPa	E/σ_y	Ultimate Tensile Strength / MPa	Elongation / %	Strain Hardening Exponent
T39	70	460	152	550	14	0.07
T351	70	360	194	535	20	0.11

Table 1- Elastic-Plastic Properties of Al2624 alloy in T39 and T351 conditions

Figure 2-3 shows the stress-strain curves for the two material, showing the difference in yield and tensile strengths. Table 1 shows the elastic-plastic properties, including the strain hardening exponent.

Table 2: Peening parameters for peening process 1 (PP1) **for Al-2624 T351 and T39 alloy systems**

Material	Power Density-Pulse duration-# Layers (GW/cm^2-ns-#)	Spot Size / mm
Al-2624 T351	1-18-1	8.5
	1-18-2	
	1-18-4	
	1-18-7	
	3-18-1	5
	3-18-2	
	3-18-4	
	3-18-7	
	6-18-1	3.5
	6-18-2	
	6-18-4	
	6-18-7	
Al-2624 T39	1-18-1	8.5
	1-18-2	
	1-18-4	
	1-18-7	
	3-18-1	5
	3-18-2	
	3-18-4	
	3-18-7	
	6-18-1	3.5
	6-18-2	
	6-18-4	
	6-18-7	

Table 3: Peening conditions for peening process 2 (PP2) for Al-2624 T351 and T39 alloy systems

Specimen #	# LAYERS	ENERGY / J	Pulse duration / ns	Power density / GW cm^{-2}	SHOTS
1-T351	1	4.9	10	2.5	4
2-T351	1	9.8	20	2.5	4
3-T351	2	4.9	10	2.5	8
4-T351	2	9.8	20	2.5	8
5-T351	2	4.9 and 9.8	BOTH 10 and 20	2.5	16
6-T351	3	9.8	20	2.5	12
7-T351	1	9.8	10	5	4
8-T351	**1**	**19.6**	**20**	**5**	**4**
9-T351	2	9.8	10	5	8
10-T351	**2**	**19.6**	**20**	**5**	**8**
11-T351	2	9.8 and 19.6	BOTH 10 and 20	5	8
12-T351	**3**	**19.6**	**20**	**5**	**12**
1-T39	1	4.9	10	2.5	4
2-T39	1	9.8	20	2.5	4
3-T39	2	4.9	10	2.5	8
4-T39	2	9.8	20	2.5	8
5-T39	2	4.9 and 9.8	BOTH 10 and 20	2.5	16
6-T39	3	9.8	20	2.5	12
7-T39	1	9.8	10	5	4
8-T39	1	19.6	20	5	4
9-T39	2	9.8	10	5	8
10-T39	2	19.6	20	5	8
11-T39	2	9.8 and 19.6	BOTH 10 and 20	5	8
12-T39	3	19.6	20	5	12

2.2 Laser peening of Al 2099 specimens

Table 4: Single Peening conditions for Al-2099 specimens

Specimen No	Extraction location	Orientation	Peening condition Single Spot
1a	Flange	yz	3-18-1
2a	Flange	xy	3-18-1
3a	Flange	zx	3-18-1
1b	Flange	yz	3-18-3
2b	Flange	xy	3-18-3
3b	Flange	zx	3-18-3
4a	Web	yz	3-18-1
5a	Web	xy	3-18-1
6a	Web	zx	3-18-1
4b	Web	yz	3-18-3
5b	Web	xy	3-18-3
6b	Web	zx	3-18-3

2.3 Cyclic Stress Strain Experiment

For the cyclic stress-strain tests, standard tensile specimens were extracted along, and across the rolling direction from both plates. The specimen geometry is shown Figure 2-4.

Cyclic stress strain tests were carried out using an Instron 3386 slow strain rate machine at room temperature. The tests were carried out in strain-control. Four specimens were extracted in the rolling direction and across the rolling direction from T351 and T39 heat treated Al-2624 plates. The specimens were cycled up to 7 cycles with a maximum strain of ±2 %.

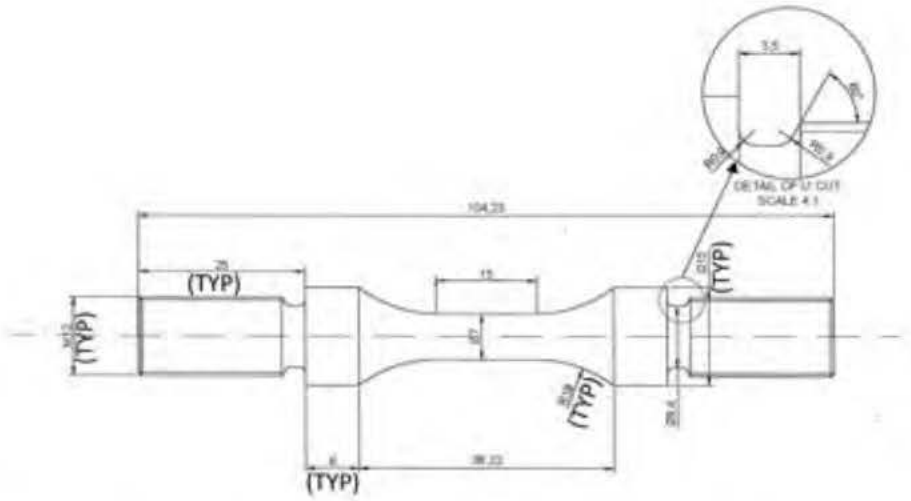

Figure 2-4: Specimen geometry used for cyclic stress-strain test. All dimensions are in mm. M12 threads were used. The dimension of the gauge length is 15 mm.

Figure 2-5: Experimental setup for cyclic stress strain test

2.4 Nanoindentation

Nanoindentation is a load- and displacement-sensing indentation technique used to determine mechanical properties of material at sub-millimetre level. Mechanical properties such as Young's modulus, yield strength, strain hardening exponent, and hardness can be estimated by this technique (Pethica 1982, Newey, Wilkins & Pollock 1982, Stone et al. 1988). The nature and magnitude of the residual macro and micro stresses can also be extracted (Suresh, Giannakopoulos 1998). This technique provides load-displacement data

from which hardness and elastic modulus are determined. For relatively soft material such as Al alloys that generate pile-up owing to plasticity during indentation, there are four methods available in the literature. They are: (1) the Oliver and Pharr method (Suresh, Giannakopoulos 1998, Oliver, Pharr 1992); (2) the Oliver and Pharr method with area correction from atomic force microscopy (AFM) (Kese, Li 2006, Beegan, Chowdhury & Laugier 2003); (3) the plastic work of indentation approach; and (4) the total work of indentation method (Tuck et al. 2001).

The Oliver and Pharr method is used in this study to determine the hardness of laser peened Al-2624 alloy. Therefore a brief summary of the theoretical background is given in the following section.

2.4.1 The Oliver and Pharr method

If a load P is applied over an area A then according to contact theory hardness can be defined as follows:

$$H = \frac{P}{A} \qquad \text{Equation 2-1}$$

The elastic modulus E of the test specimen can be determined from the reduced modulus, E_r which is related to elastic contact stiffness, S, and indenter geometry constant, β according to the following equation:

$$E_r = \frac{\sqrt{\pi} \bullet S}{2\beta \sqrt{A}} \qquad \text{Equation 2-2}$$

The elastic modulus of the specimen, E, can then be determined from the following equation:

$$\frac{1}{E_r} = \frac{(1-\nu^2)}{E} + \frac{(1-\nu_i{}^2)}{E_i} \qquad \text{Equation 2-3}$$

Where ν and ν_i are the Poission's ratios of the specimen and indenter respectively, and E_i is the Elastic modulus of the indenter. For Berkovich type triangular indenters, β = 1.034.

The projected contact area, A, can be empirically determined from the area function at the contact depth, h_c:

$A=f(h_c)$ **Equation 2-4**

The contact depth h_c is related to the total depth, h, according to the following equation

$$h_c = h - \varepsilon \frac{P}{S} \qquad \text{Equation 2-5}$$

Where S is the contact stiffness and ε is the indenter geometry constant. For Berkovich and cone indenters ε = 0.75 and 0.72 respectively.

The contact stiffness can be obtained by differentiating the power law equation proposed by Oliver and Pharr model.

$$P = B(h - h_f)^m \qquad \text{Equation 2-6}$$

Where h and h_f are respectively the resultant penetration and the final displacement after complete unloading; B and m are the fitting parameters.

And thus

$$S = \frac{Bm(h-h_f)^{m-1}}{h=h_{max}} \qquad \text{Equation 2-7}$$

A schematic representation of the indentation process is given in **Figure 2-6**

All indentations experiments were carried out using an MTS Nanoindenter® XP system with a Berkovich indenter tip.

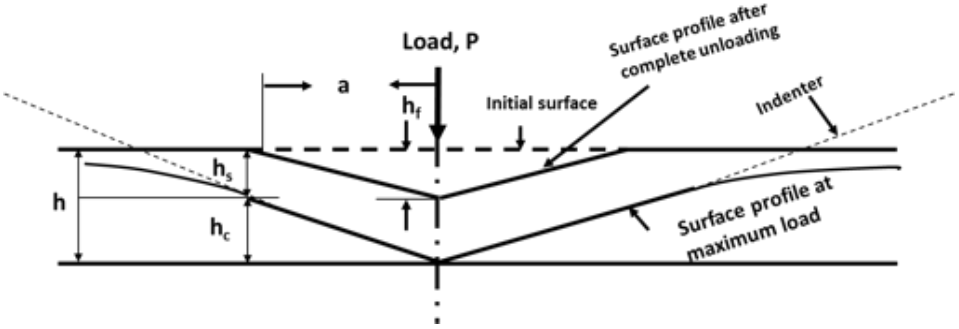

Figure 2-6: Schematic of the indentation process

2.4.2 Indentation procedure

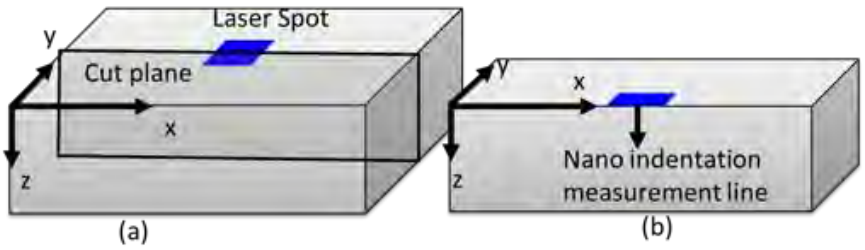

Figure 2-7: Schematic representations of (a) nanoindentation specimen preparation and (b) measurement line with respect to the cross-sectional area.

All specimens were EDM cut along the centreline of the laser spot, mounted in resin and metallographically prepared. Figure 2-8(a) shows a schematic representation of the EDM cut and the measurement line with respect to the cross-section of the specimen. For each specimen two lines of 70 indents each were made with 100 µm spacing between the indents. The instrument was operated in basic hardness load-displacement mode that records load, displacement and time. In order to calculate the hardness contact stiffness needs to be measured. Therefore, the indentation measurement was performed with the "Continuous Stiffness Measurement" option that allows continuous measurement of the contact stiffness during loading. Specimens were tested with 20 mN and 50 mN load: however, only results for 50 mN load are presented here. There was no difference in the results from the two load levels used.

2.5 Incremental Hole Drilling

Hole drilling is a relatively fast, relatively straightforward, and inexpensive method for residual stress measurement in the laboratory. As the name implies, in this technique a hole is drilled into the specimen to cause elastic stress relaxation as material is removed. The elastic stress relaxation causes a change in displacement in the surrounding material that is measured by the strain gauge attached to the specimen (see **Figure 2-8**). The residual stresses are then calculated from the measured displacements.

Laser peening generally introduces a deep compressive residual stress with a relatively steep stress gradient. Therefore, holes were drilled in small increments so that a depth profile could be obtained. Hole drilling measurement was carried out using a set up developed by Stresscraft, UK. For an accurate measurement the UK NPL Good Practice

Guide No. 53 and standard ASTM 837 were followed (Grant, Lord & Whitehead 2006). A 2-mm-diameter hole was drilled in an orbital motion with four increments of 32 μm, four increments of 64 μm, and eight increments of 128 μm: a total of 16 increments to a total depth of 1.4 mm.

Figure 2-8: Experimental setup for hole drilling measurement

2.6 Texture measurement using neutron diffraction

The crystallographic orientation of the extruded Al-2099 alloy was measured using neutron diffraction at the GEM instrument at the UK's ISIS neutron source (Kockelmann, Chapon & Radaelli 2006). GEM is used to characterize texture in materials. Six detector banks comprising 700 individual detectors as shown in Figure 2-10a provide considerable coverage in orientation space. Each detector group covers approximately 10° × 10°.

A total of seven specimens with dimensions 5 × 5 × 2 mm³ were extracted from the web and flange sections of the extruded T-bar (see Figure 2-9) to study the texture variation at these locations. A beam size of 20 × 20 mm² was used. Data sets were collected at a 0° rotation position only. The recorded data in 164 detectors corresponding to the detector grouping were normalized to the incident neutron flux distribution, corrected for detector efficiencies, and converted to diffraction pattern (intensity as a function of *d*-spacing). The diffraction patterns were then Rietveld fitted (Wenk, Lutterotti & Vogel 2010) in MAUD software (Lutterotti et al. 1997). (111), (200) and (220) pole figures were plotted. An example of the fitted spectra is shown in Figure 2-11.

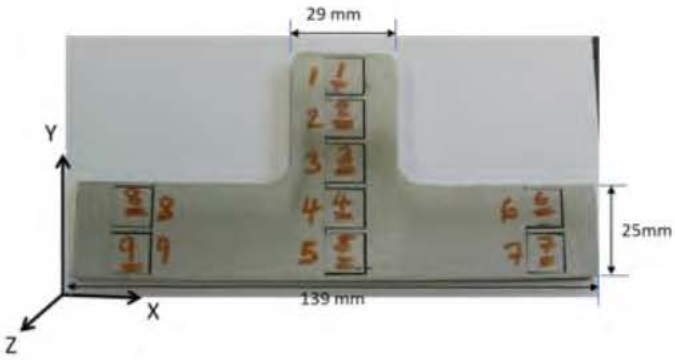

Figure 2-9: Extruded 2099 bar

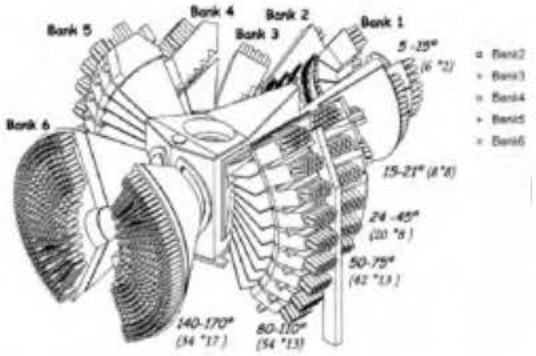

(a)

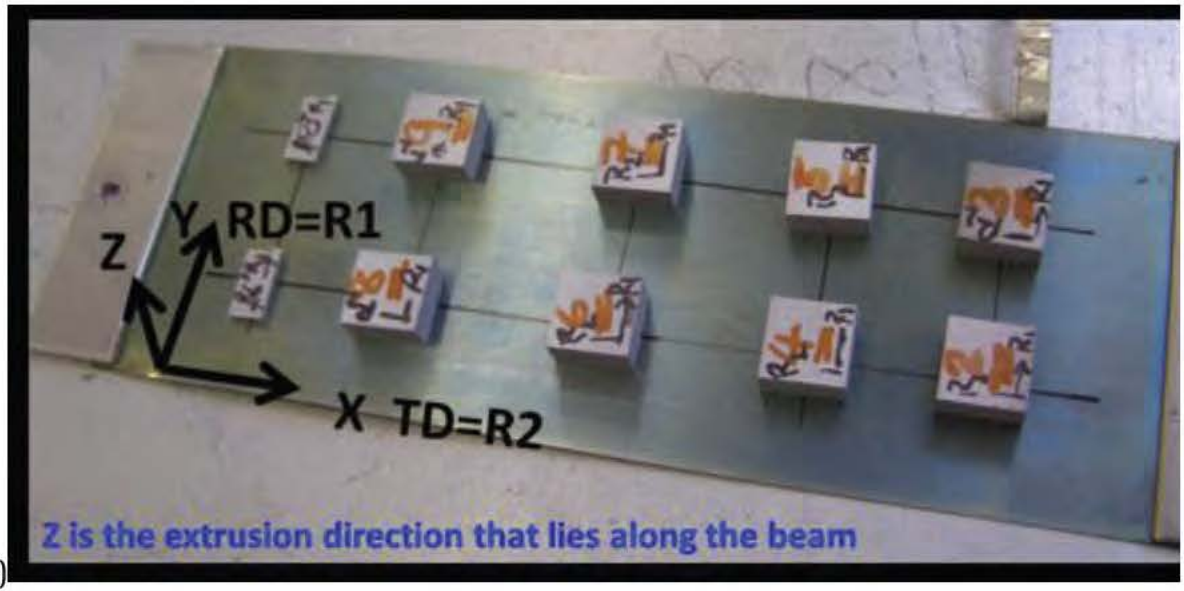

(b)

Figure 2-10: (a) GEM detector arrays and pole figure coverages {Kockelmann,W. 2006}; (b) the specimen arrangement on the aluminium sample holder.

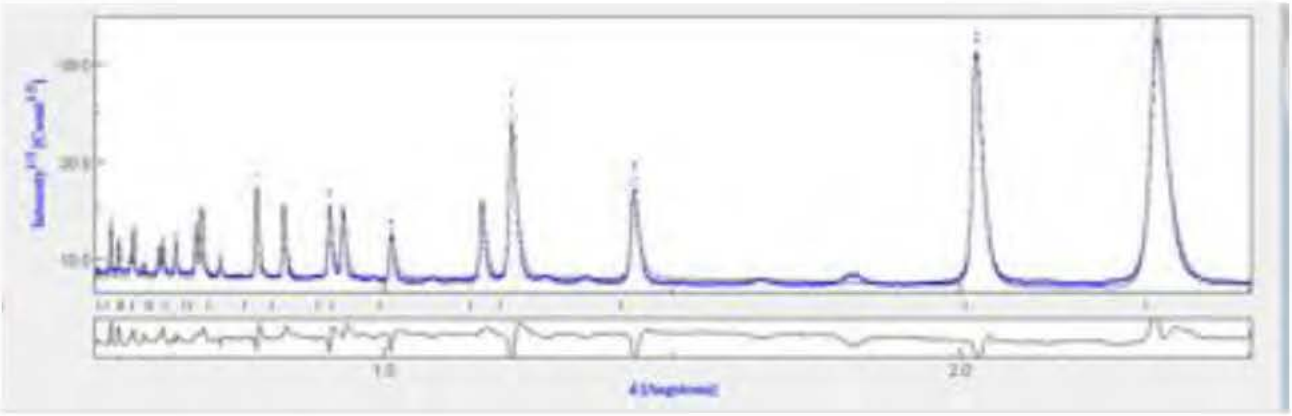

Figure 2-11: Neutron diffraction spectra fitting in MAUD software

Chapter 3. Results and discussion: Al-2624

3.1 Cyclic Stress Strain Behaviour of Al-2624

Figure 3-1a and b show the cyclic stress-strain behaviour of Al-2624 T351 and T39 that have yield strengths of 350 and 430 MPa respectively. After four cycles the T39 alloy seems to reach saturation, whereas T351 gradually hardens up to the 7th cycle.

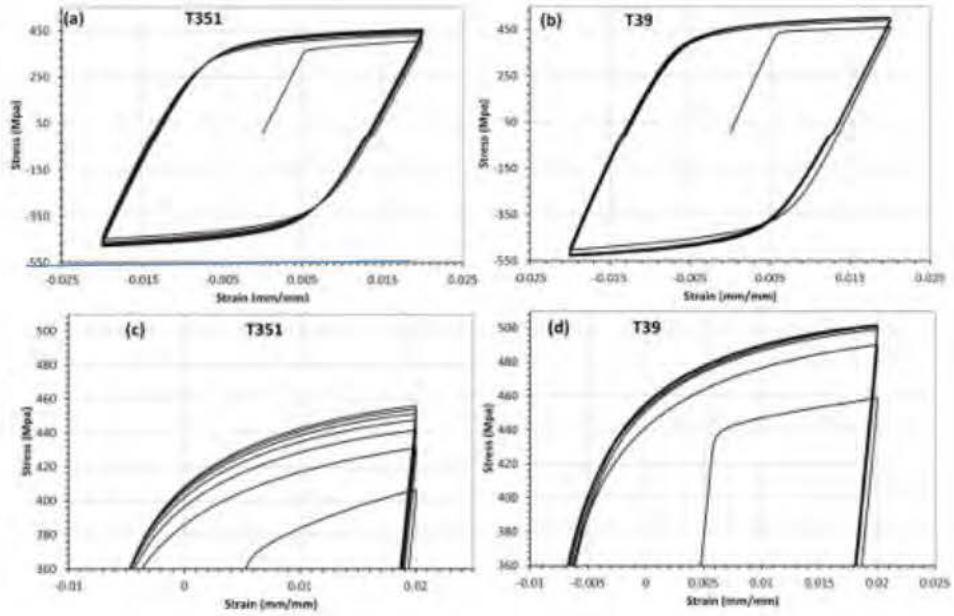

Figure 3-1: Cyclic stress-strain curve for Al-2624 alloy for 7 cycles (a) for T351 alloy and (b) T39 alloy. Tests were carried out under strain control to ±2 % strain. (c) and (d) shows details of the plastic behaviour in tensile loading.

Figure 3-1c shows a schematic representation of a typical metallic stress-strain response. Figure 3-1d and 3-1e show details for the 2624 heat treatments.

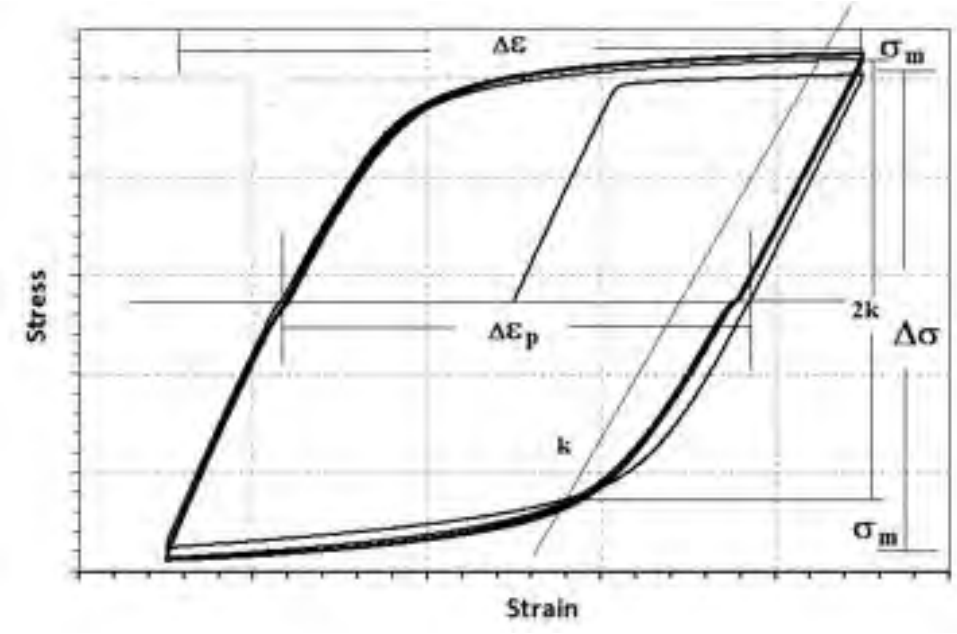

Figure 3-1c: Schematic of the cyclic stress-strain response

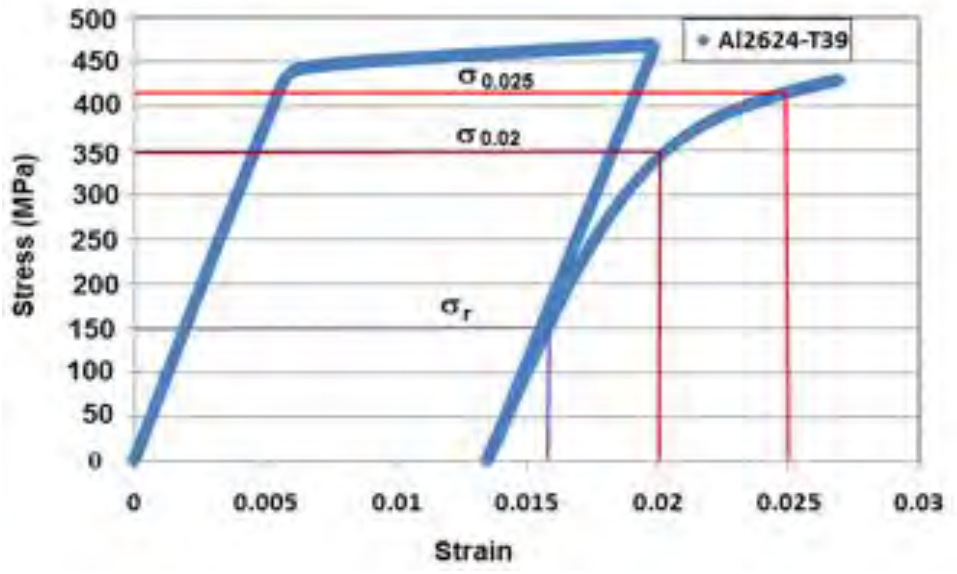

Figure 3-1d: Detail of cyclic Stress-Strain curve for Al 2624 T39

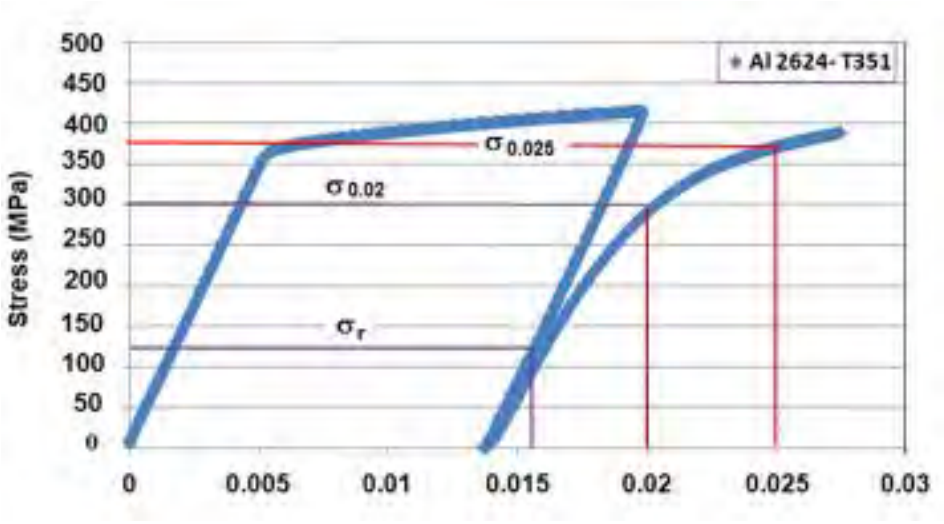

Figure 3-1e: Detail of cyclic Stress-Strain curve for Al 2624 T351

The stress, strain and associated parameters are used to define the reverse yielding or Bauschinger effect phenomenon. The Bauschinger parameters are calculated from the cyclic stress-strain response and are shown in Table 3-1. $\beta_{\sigma 1}$ shows the relative decrease in the yield stress from forward to reverse deformation, termed as short range work softening while $\beta_{\sigma 2}$ and $\beta_{\sigma 3}$ are the restoration of the yield stress and are termed as long range work softening. Table 3-1 shows the cyclic stress-strain parameters obtained for the alloy in both conditions. It can be seen the alloys show similar behaviour in cyclic loading.

Heat Treatment	$\varepsilon_t = \varepsilon_{el} + \varepsilon_p$	$\frac{\Delta\varepsilon_{pl}}{2}$	$\beta_{\sigma 1}$	$\beta_{\sigma 2}$	$\beta_{\sigma 3}$
T39	0.02	0.027	0.67	0.24	0.098
T351	0.02	0.028	0.69	0.27	0.096

Table 3-1: Cyclic Stress-Strain properties of Alloy 2624 in T39 and T351 conditions

3.2 Surface profiles

The surface profile caused by laser peening was measured by a Leica Microsystems Laser Confocal Microscope. Figure 3-2 shows the 2D surface profile for T351 with conditions 6-18-4 (Power density – pulse duration – number of layers). In order to compare the depression between different peening conditions line profiles were taken along a horizontal axis and the results are presented in Figure 3-3. For 1 GW/cm^{2,} specimens 1-18-1 (S-1) and 1-18-7 (S-4) the depression increased with the number of peening layers. Interestingly,

when the energy was increased by 3 times, for a single peening layer 3-18-1 a similar depression was observed as for seven shots at the lower power density (1-18-7). Figure 3-3b shows the comparison of line profiles between specimen 6-18-2 (S-10) and 6-18-7 (S-9). 1 At 6 GW/cm^2, the depression depth after 2 and 7 layers is 40 and 100 µm respectively. The bottom surface of the depression created by the laser shock is not uniform. Also Figure 3-3b shows material pile-up at the edges of the depression. The specimen that was hit twice showed pile-up of 40 µm close to the edge, whereas 7 hits generated a much larger pileup (110 µm on one side and 80 µm on the other side). The hardness and residual stress measurements carried out on these specimens are presented in section 3.3 and 3.4 respectively.

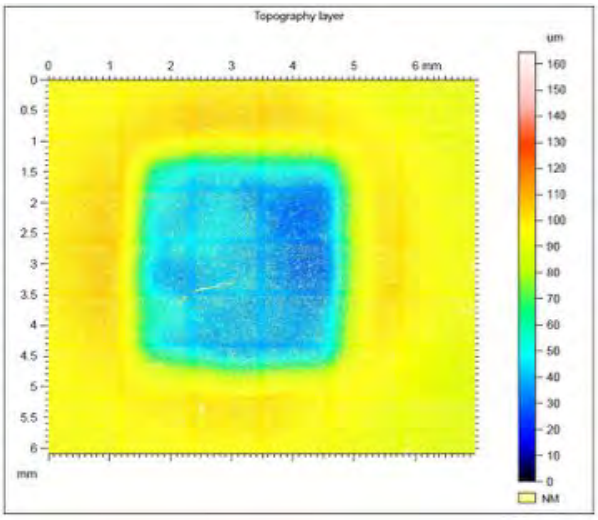

Figure 3-2 2D surface profile of specimen T351 3-18-4

(a)

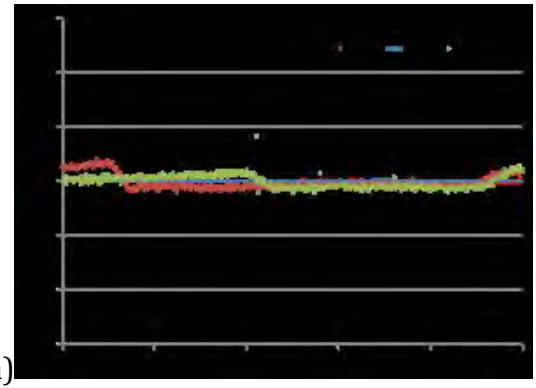

(b)

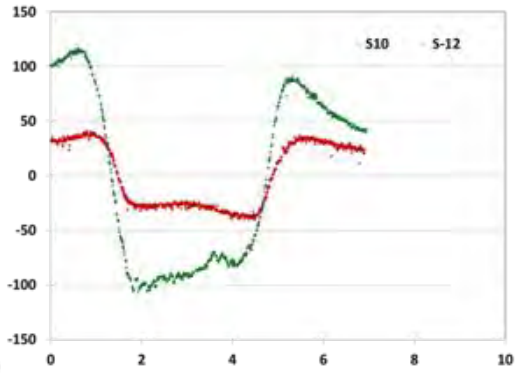

Figure 3-3: Comparison of line profiles along a horizontal axis (a) for specimen S-1(1-18-1), S-4 (1-18-7), and S-5 (3-18-1), and (b) for specimen S-10 (6-18-2) and S-12 (6-18-7).

3.3 Hardness results measured by nanoindentation

20 and 50 mN loads were used for hardness measurement with two lines of 70 indents made at each load. Figure 3-4 shows the indentations for T31 and T39 conditions.

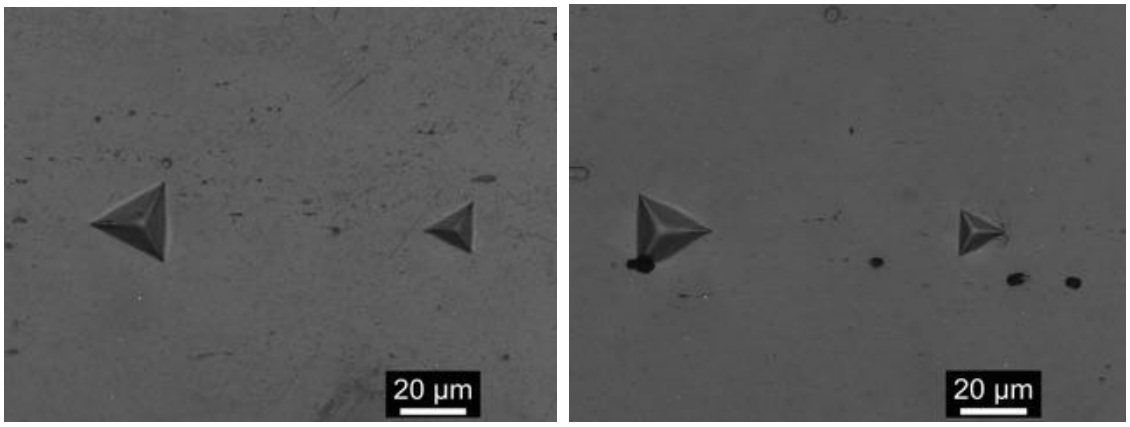

Figure 3-4: Scanning electron micrographs for T351 (left) and T39 (right) alloys showing the indents

3.3.1 Effect of Power Density (PP-1) with 18 ns shot duration

Figure 3-5 presents normalized hardness results as a function of depth below the surface after 1 layer at power densities of 1, 3, and 6 GW/cm^2 for (a) T351 and (b) T39 alloy. It is evident that the hardness values increase with increasing power density for both heat treatments. It is interesting to note here that for 6 GW/cm^2 after the first shot T351 was hardened by up to 10% whereas for T39 15% hardness increase is observed. The T39 material would be expected to show a lower hardening ratio compared to T351 for similar conditions.

In order to investigate the hardening response between the two alloys the effect of power density after 7 layers was also studied. Figure 3-5 c and d show the effect of power density for T351 and T39 alloys respectively. Hardness values continue to increase for T351 alloy with increasing power density from 1 to 6 GW/cm^2. However, for the T39 alloy the hardness values slightly dropped for the higher power densities, perhaps reflecting some reverse yielding near-surface. The effect of number of layers on the hardening response is further discussed in section 3.3.3.

Another important feature that can be observed from this plot is the affected depth from the peening. For T351 the affected depth is ~2 mm with no change with increasing energy. However, after 7 hits this depth was increased to ~2.5 mm. In the T39 alloy the affected depth after for 1 shot is 2.5 mm which remained unchanged with increasing energy and number of layers.

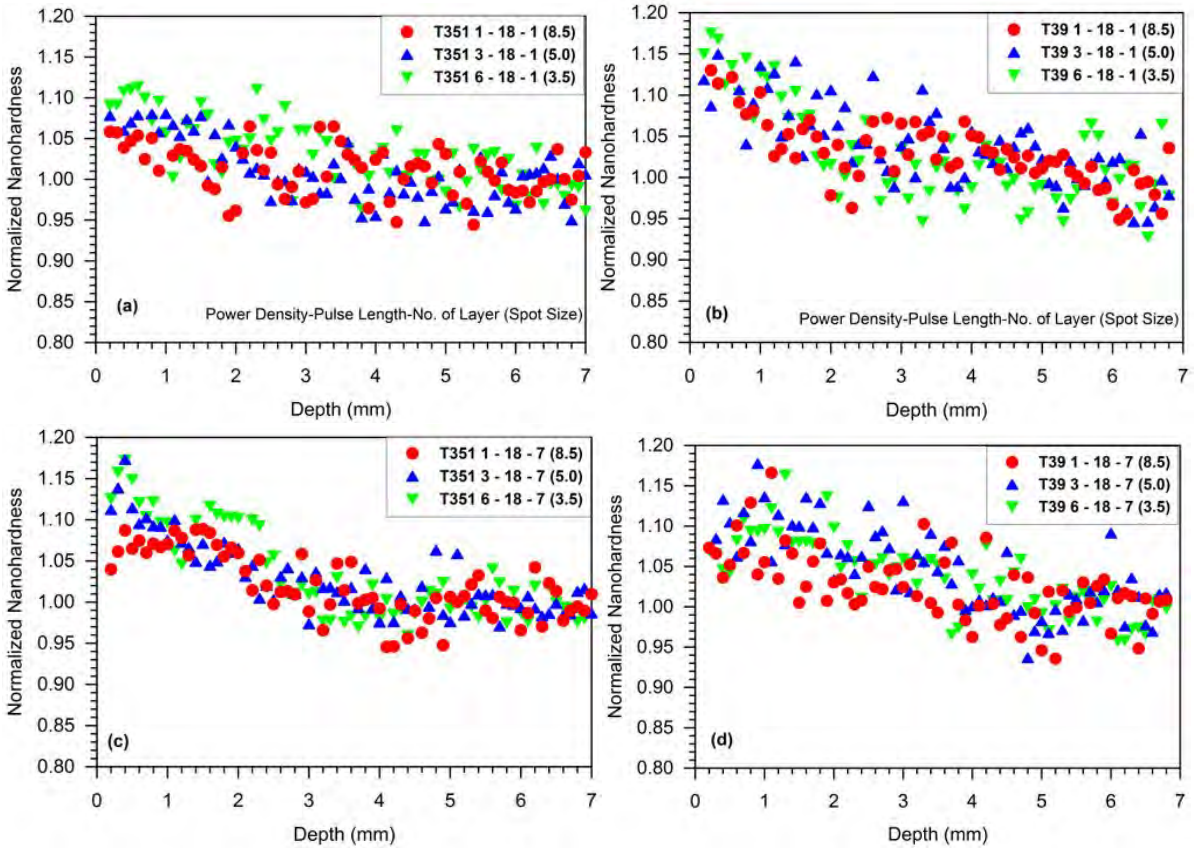

Figure 3-5: Effect of power density on the hardness of (a) T351 alloy and (b) T39 alloy after 1 shot; and (c) T351 alloy and (d) T39 alloy after 7 shots.

3.3.2 Effect of Power Density (PP-2)

Power density again has a marked effect on the hardness response of the material. The effect of power density on the hardness (normalised with respect to the hardness at the unaffected zone) is presented in Figure 3-6 for 2.5 and 5 GW/cm^2 after 3 layers for (a) T351 and (b) T39 alloy. A slight hardness increase can be observed for T351 alloy when the energy was doubled. In contrast, no hardness change can be observed for T39 alloy.

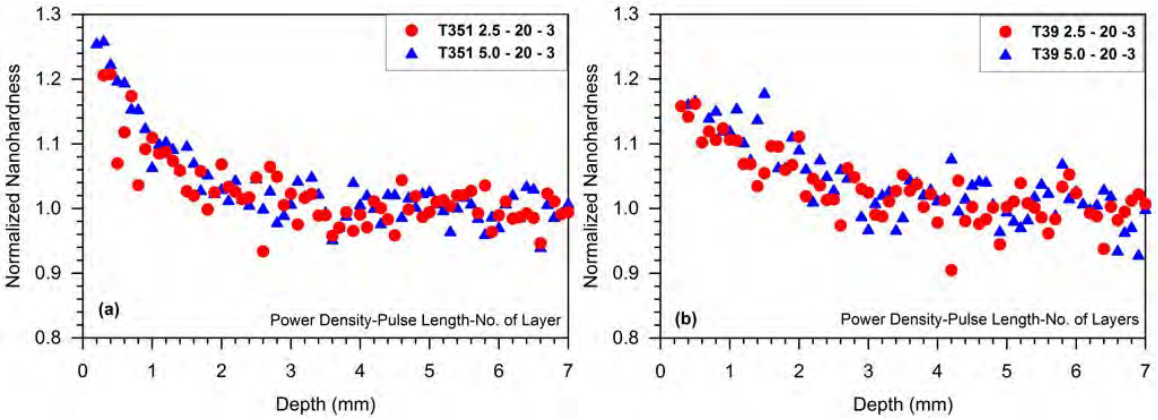

Figure 3-6: Effect of power density on the hardness of specimens processed by PP2 for (a) T351 alloy and (b) T39 alloy after 3 shots.

3.3.3 Effect of number of layers (PP-1)

The effect of number of peening layers on the hardness was studied in specimens peened at power densities of 1, 3, and 6 GW/cm^2. A large scatter in the hardness results was observed in the specimens peened at 1 GW/cm^2. No discernible trend could be identified. Therefore, the results are omitted here.

Figure 3-7 a and b show the normalized hardness profile as a function of depth at 3 GW/cm^2 for 1, 2, 4 and 7 layers for T351 and T39 alloy respectively. Hardness was increased by 8% compared with the unaffected area after one shot. A further 12% hardness increase was observed after four shots. No further hardness increase was obtained for 7 shots. For T39 alloy a 12% hardness increase was obtained after the first shot and no further change was evident following additional shots.

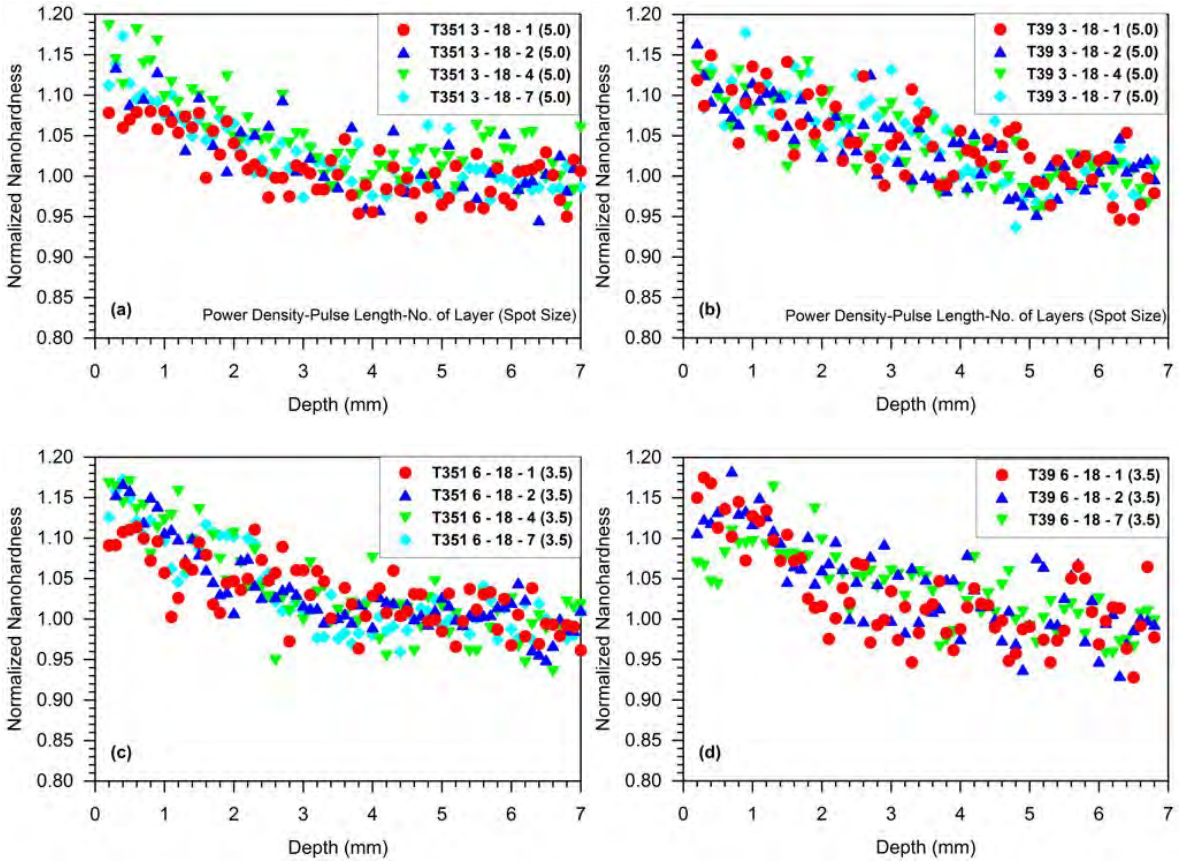

Figure 3-7: Effect of number of peening layers on the hardness of (a) T351 alloy and (b) T39 alloy at 3 GW/cm²; and (c) T351 alloy and (d) T39 alloy peened with a power density of 6 GW/cm².

When the power density was doubled an interesting difference in hardening response was observed between two alloys. At 6 GW/cm² 10% hardening was observed (Figure 3-7c) after the first shot in T351, that increased to 15% after the 2nd shot. However, no further increase was evident in the subsequent 4 and 7 layers. By contrast 15% hardness increase was seen for the T39 alloy (see Figure 3-7d) after the first shot and with additional hits the material seemed to be softened slightly near the surface which is either a consequence of the Bauschinger effect or indicative of micro-cracking in the sample with repeated high-energy shocks. The affected depth owing to peening in the T39 alloy is 1 mm greater than the T351 alloy at 3 GW/cm². For 6 GW/cm² the affected depth for both alloys is 3 mm. Comparison of the affected depth between the two power densities shows that a higher depth was obtained at 3 GW/cm². It is important to note here that the spot size at 3 GW/cm² was 5 × 5 mm² whereas the spot-size for the specimen peened at the highest

power density was 3.5 × 3.5 mm^2. In combination with the softening effect that is evident for T39 alloy at highest energy, the affected depth is also less.

3.3.4 Effect of number of layers (PP-2)

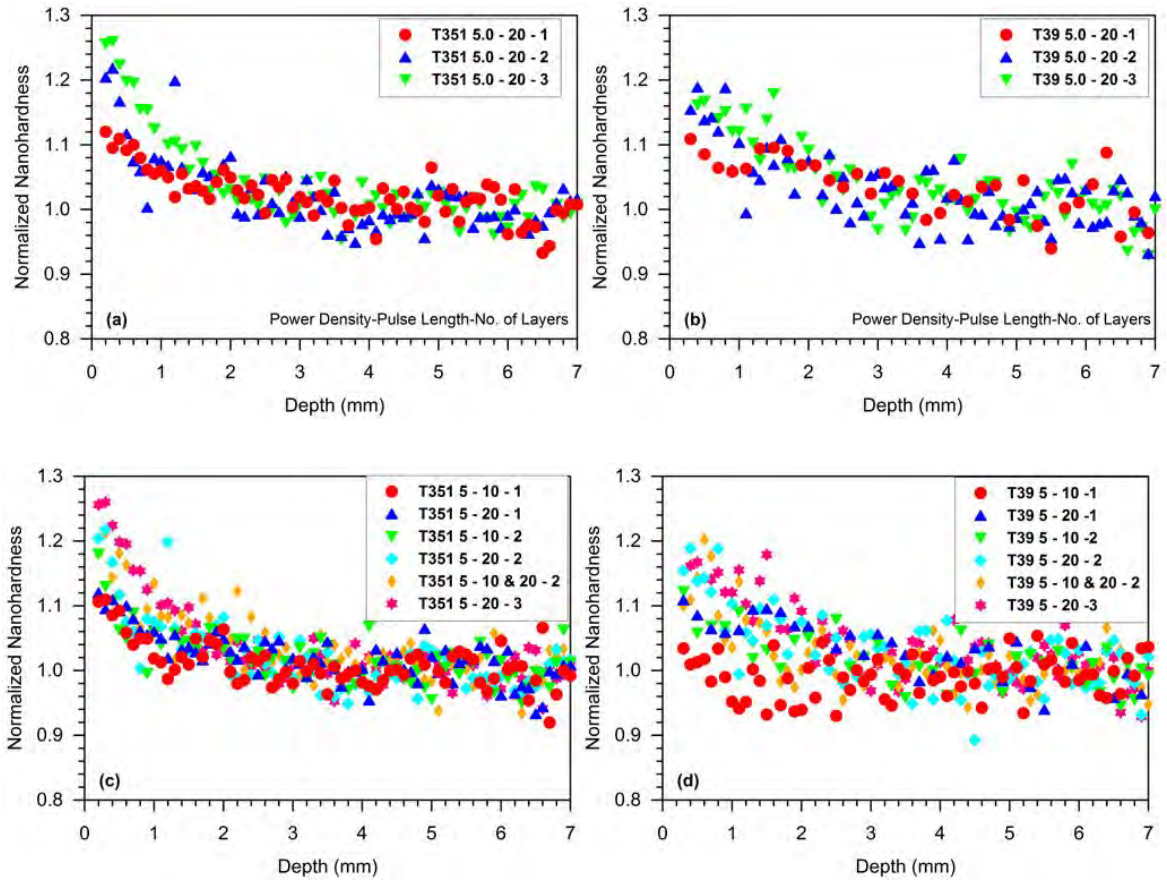

Figure 3-8: Effect of number of peening layers (1, 2 and 3) on the hardness for (a) T351 alloy and (b) T39 alloy. (c) T351 alloy and (d) T39 alloy for various peening treatments. The specimens were peened with a power density of 5 GW and a pulse width of either 10 or 20 nanoseconds.

For peening process 2 (PP-2) the effect of number of layers on the hardness is shown in Figure 3-8 a and b for T-351 and T39 respectively. Again, for the T351 alloy a 10% hardness increase was observed after the first shot at power density of 5 GW/cm^2, which is then increased to 20% after the 2nd layer and finally 25% after the 3rd layer. For this alloy the affected depth does not change with number of layers. There is an interesting effect in that the affected depth seems to be relatively shallow (only 1.5 mm) in comparison to PP-1 (see Figure 3-8). This is notable because it implies that for a similar energy input to the sample, at similar power densities and pulse length, different hardening effects can be achieved. The different methods may lead to different pressure pulse profiles into the sample, and this is an area for future study.

For the T39 alloy 10% hardness increase can be seen after the first layer, increasing to 18% after the 2nd layer with no further change evident after the 3rd layer. The affected depth is ~2 mm. Figure 3-8c suggests that in that T351 alloy the hardness continued to increase with increasing number of layers and energy. The maximum hardness is ~1.25 times the unpeened hardness, whereas for T39 alloy (Figure 3-6 d) the maximum hardness is ~1.2 times the unpeened hardness values.

3.3.5 Correlation between the two peening processes

Although the processing techniques used in PP1 and PP2 are not exactly the same, comparison has been made between two processes as shown in Figure 3-9 (a) for T351, and (b) T39. In peening process 1 the highest power density used was 6 GW/cm^2 whereas for PP2 the highest energy used was 5 GW/cm^2 with a slightly longer (20 ns) pulse duration, which is a difference in energy input of less than 10%. No significant difference between the hardening response of either alloy could be identified. This indicates that a similar material response can be expected for a similar peen energy input with similar conditions.

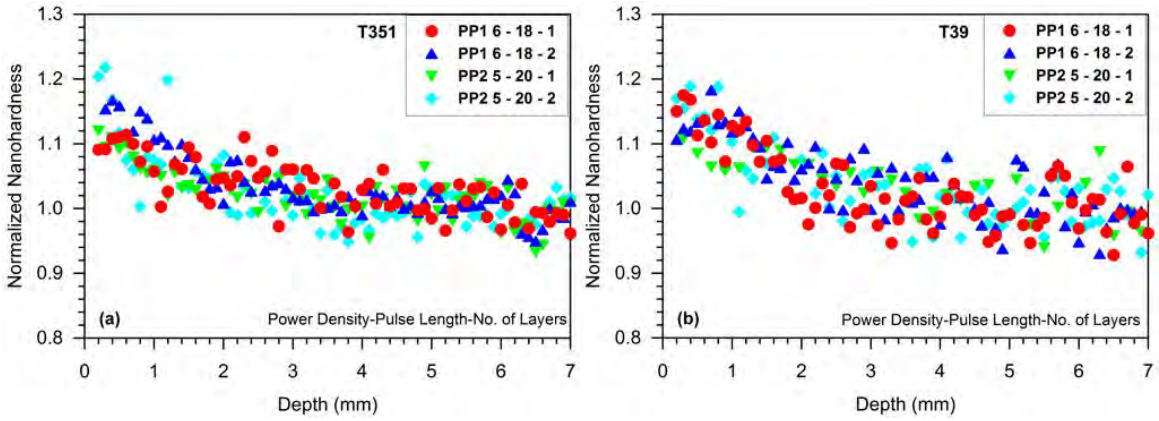

Figure 3-9: Comparison between two peening process studied here showing the effect of energy after 1 layer and two layers for (a) T51 alloy and (b) T39 alloy.

3.4 Residual Stress

The observed hardness increase may be a combined effect of the residual stress associated with the LSP process and material's intrinsic hardening response. Although established methods are available in the literature to extract residual stress from nanoindentation load-displacement data (Suresh, Giannakopoulos 1998, Khan et al. 2011), separate techniques

for residual stress characterisation were employed in the current study, and the results are presented in the following sections.

3.4.1 Incremental Hole drilling

The near-surface residual stress distribution was determined using incremental hole drilling technique in as-received material, and after the EDM surface preparation prior to peening. The specimens were prepared using the EDM machine in skim cut settings (comprising four cuts) in order to obtain a fine surface finish (surface roughness, R_a = 1). As shown in Figure 3-10 the near surface residual stress in as-received material is around 30 MPa tensile, and that of the surface after EDM is about 80 MPa compressive.

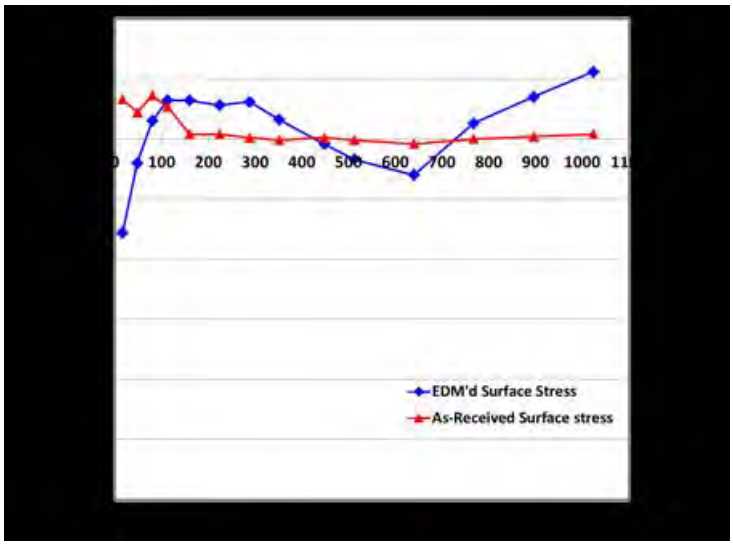

Figure 3-10: Surface residual stress distribution as a function of depth in Al2624 T351 alloy in as-received and EDM'd surfaces before peening.

The residual stress distribution measured by incremental hole drilling is presented in Figure 3-11 (a) for Al2624 T351 specimens peened with 1 GW/cm^2 with 1, 2, 4 and 7 layers. For the T351 alloy, after 1 shot a maximum compressive residual stresses of –195 MPa was obtained at a depth of 48 µm. For 2 layers and 4 layers no significant change in the residual stress profile is observed, however, the maximum compressive residual stresses are slightly deeper. After 7 shots the highest surface compressive residual stress is –250 MPa and maximum compressive residual stress –255 MPa at 112 µm depth. The overall shape of the residual stress profiles of the four different layers looks similar.

Residual stresses at 3 GW/cm^2 and 6 GW/cm^2 for different numbers of peening layers are given in Figure 3-11 b and c respectively. At both power densities, the magnitude of

compressive residual stress increases with increasing number of layers from 1 to 4 layers. However, at the highest energy used here the near-surface residual stress relaxation took place, which is almost certainly a consequence of reverse yielding of the material.

Figure 3-12a shows an apparent anomaly in the results for 1-18-1 compared to the other conditions. However, the results for this condition were validated by laboratory X-ray diffraction as below.

Direction	XRD Residual Stress / MPa	Hole Drilling Residual Stress / MPa
RD	–197	–219
TD	–239	–248

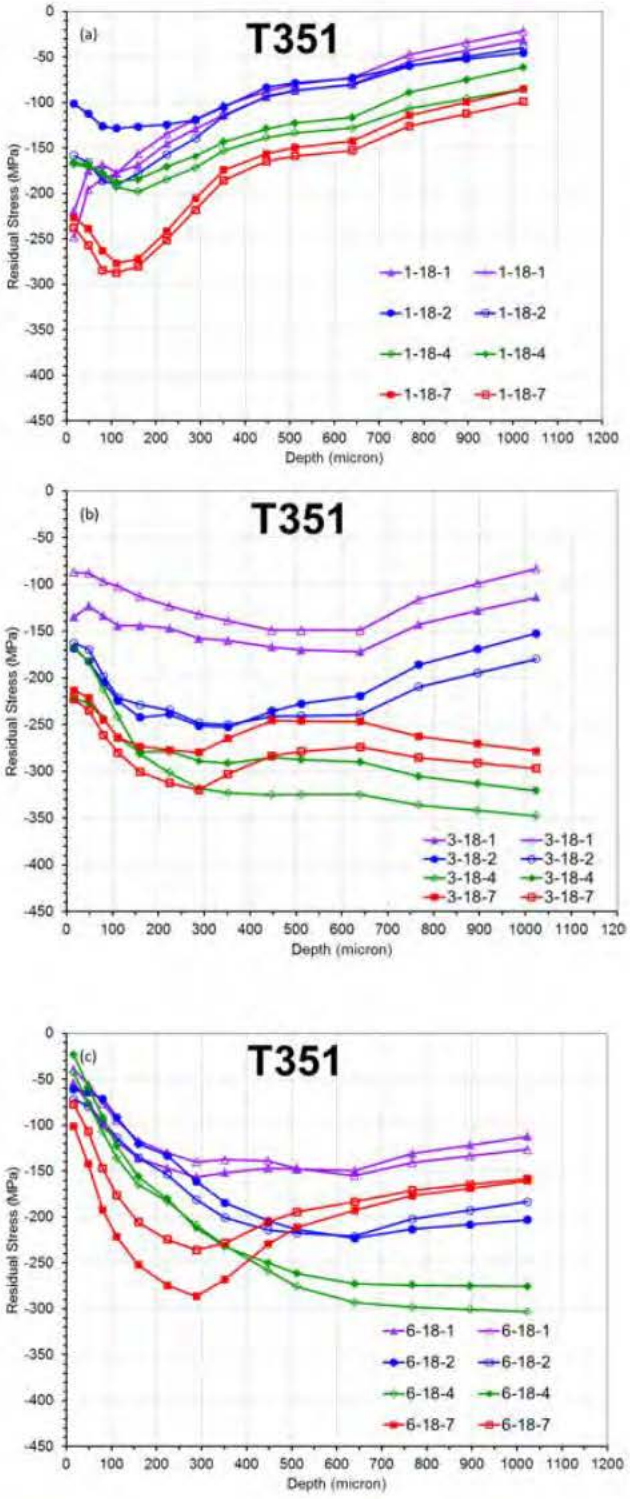

Figure 3-11: Residual stress profiles measured by incremental hole drilling showing the effect of number of layers in T351 alloy at: (a) 1 GW/cm² (b) 3 GW/cm², and (c) 6 GW/cm²

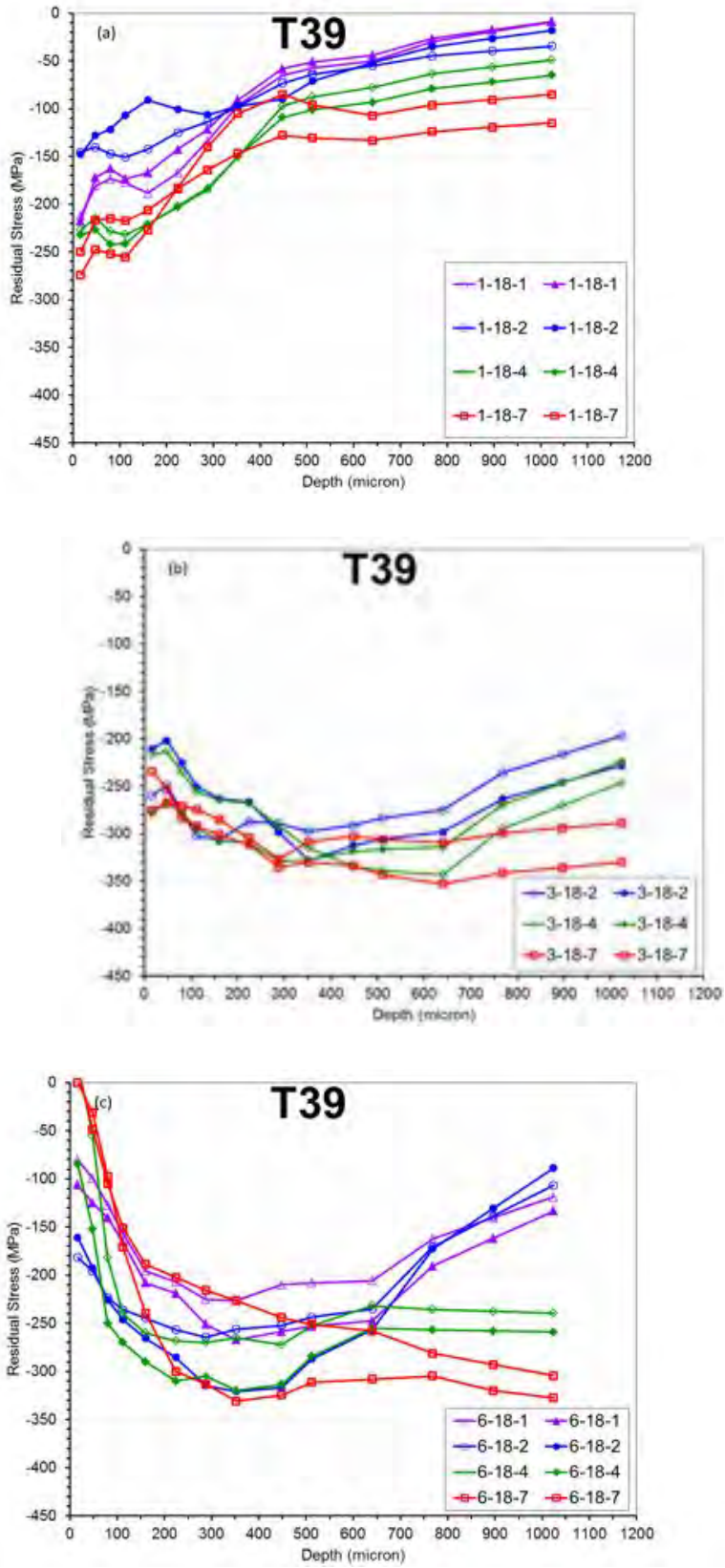

Figure 3-12: Residual stress profiles measured by incremental hole drilling showing the effect of number of layers in T39 alloy at: (a) 1 GW/cm² (b) 3 GW/cm², and (c) 6 GW/cm²

Figure 3-12 a, b and c show the residual stress distribution in Al-2624 T39 for peening at 1, 3, and 6 GW/cm^2 after 1, 2, 4 and 7 layers. The maximum compressive residual stresses occurred at the surface for 1-7 layers at 1 GW/cm^2. For 6 GW/cm^2, lower compressive stresses were found near the surface, probably due to reverse yielding.

The comparison of residual stress between the two heat treatment conditions is shown in Figure 3-13 (a) for 1GW/cm^2 and (b) for 6 GW/cm^2. Similar l residual stresses were generated for peening at 1 GW/cm^2, however, a dramatic difference in residual stress is evident for 6 GW/cm^2 after 1 layer. The value of maximum compressive residual stresses nearly doubled in the T39 alloy compared to T351. This can be related to the higher yield strength and UTS of the T39, and so an ability to generate higher residual stresses.

Table 1: Residual stresses for laser peened Al2624 T351 and T39 alloy measured by incremental hole drilling. In this Table Surface Residual Stress is the stress at a depth of 48 µm from the surface. The maximum value (between the two in-plane directions measured) of the compressive residual stresses are used in all cases

T351			
Specimen (GW/cm^2 -ns- #Layer)	Surface residual stress / MPa	Maximum Compressive Residual Stress / MPa	Residual Stress at 1 mm depth / MPa
1-18-1	–195	–195 at 48 µm	–30
1-18-2	–165	–190 at 112 µm	–45
1-18-4	–170	–195 at 160 µm	–80
1-18-7	–255	–285 at 112 µm	–95
3-18-1	–120	–172 at 640 µm	–110
3-18-2	–180	–250 at 352 µm	–180
3-18-4	–222	–323 at 352 µm	–347
3-18-7	–230	–320 at 288 µm	–295
6-18-1	–75	–156 at 288 µm	–126
6-18-2	–80	–220 at 512 µm	–200
6-18-4	–75	–300 at 896 µm	–300
6-18-7	–141	–286 at 288 µm	–158

T39			
Specimen (GW/cm^2- ns-#Layer)	Surface residual stress / MPa	Maximum Compressive Residual Stress / MPa	Residual Stress at 1 mm depth / MPa
1-18-1	–180	–188 at 160 µm	–9
1-18-2	–140	–145 at 80 µm	–35
1-18-4	–220	–240 at 80 µm	–65
1-18-7	–250	–255 at 112 µm	–110
3-18-1			
3-18-2	–260	–327 at 352 µm	–228
3-18-4	–232	–286 at 640 µm	–205
3-18-7	–265	–350 at 640 µm	–170
6-18-1	–120	–265 at 352 µm	–130
6-18-2	–190	–320 at 352 µm	–100
6-18-4	–150	–320 at 352 µm	–260
6-18-7	–100	–330 at 288 µm	–330

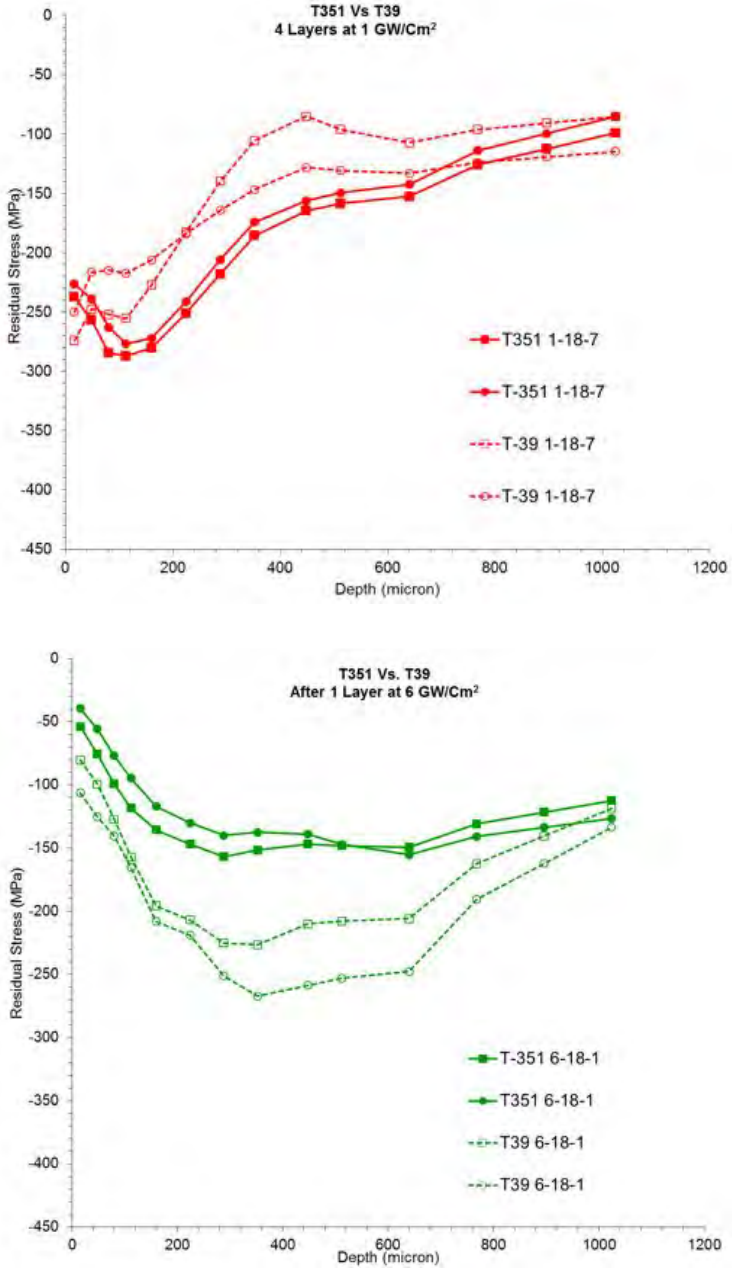

Figure 3-13 Residual stress distributions measured by incremental hole drilling

3.5 Conclusions on hardening behaviour

The two peen processes applied here showed comparable effects on the hardening of the two materials, indicating that the primary factors in hardening the material are the energy and associated power density. Some difference was observed in the depth affected by the process, and this would merit further study.

The work hardening exponent of the T39 condition was lower than the T351 condition. In peening, the T39 condition alloy owing to its lower capability to harden showed a lower increase in hardness as compared to T351 condition alloy. It could be said that in the T39 condition the alloy is therefore more responsive to peen with lower power density or fewer layers. Repeated peening may not produce any further hardening in the T39 material, potentially leading instead to the formation of micro-cracks in the material.

Figure 3.14 shows the effect of the power density and number of peen shocks on the hardness for the T351 alloy, and Figure 3.15 for the T39, for process 1.

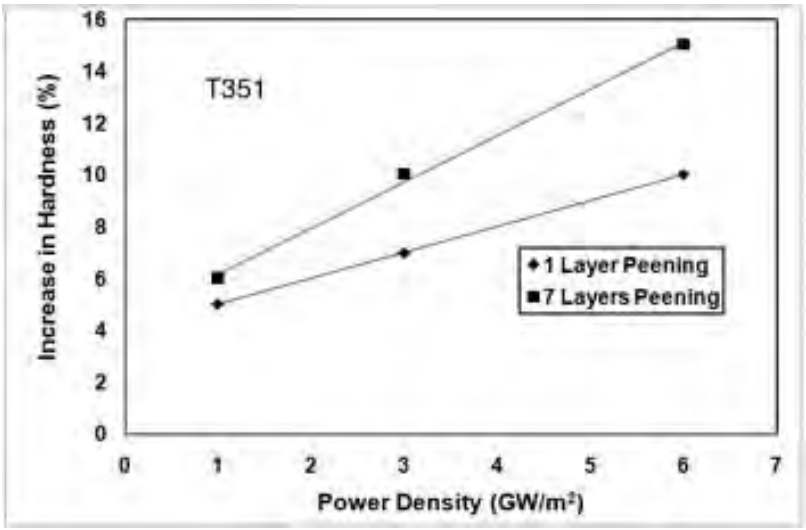

Figure 3.14: Effect of the power density and the number of peen shocks on the hardness for the T351 alloy

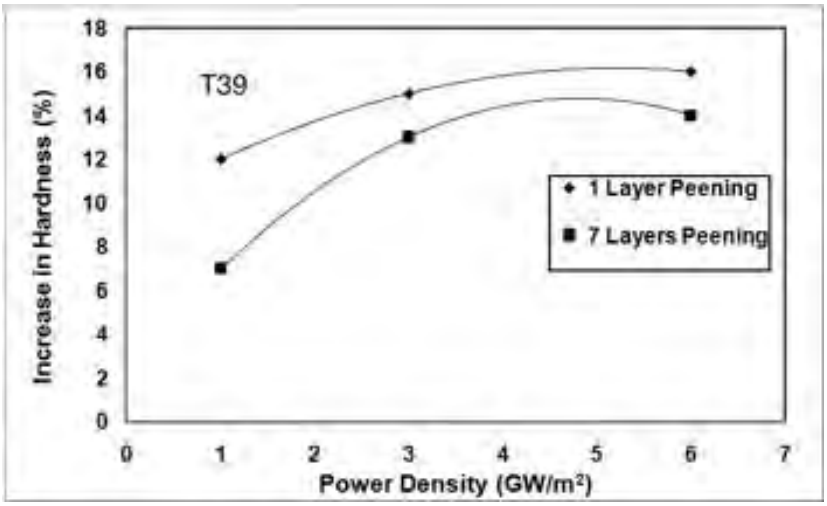

Figure 3.15: Effect of the power density and the number of peen shocks on the hardness for the T39 alloy

For the T351 there is an increase in hardness with increasing power density up to 6 GW/cm^2, whilst the T39 effectively saturates after 3 GW/cm^2, reflecting the lower work hardening capacity for that heat treatment. This is illustrated further for the two materials by Figure 3.16

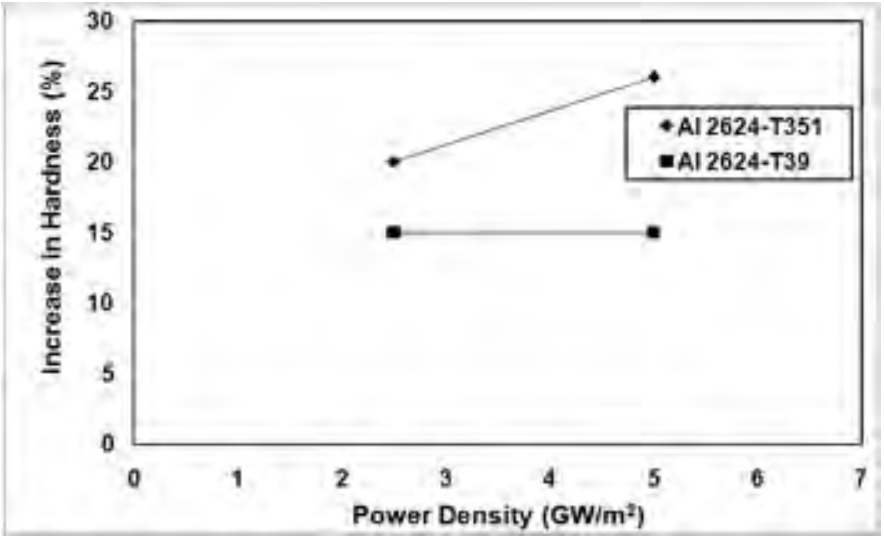

Figure 3.16: Change in hardness with power density for the two alloy conditions

The two tempers showed different response to the number of peen layers. Figure 3.17 shows the response for the T351, where an increase up to four layers is seen but then a slight decrease when seven layers are applied, for both 3 and 6 GW/cm^2. For the T39 condition (figure 3.18) the response is quite different: at 3 GW/cm^2 there is a slight increase

in hardness with number of layers, but at the higher power density of 6 GW/cm^2 there is a steady drop in hardness, probably from reverse yielding and cyclic softening.

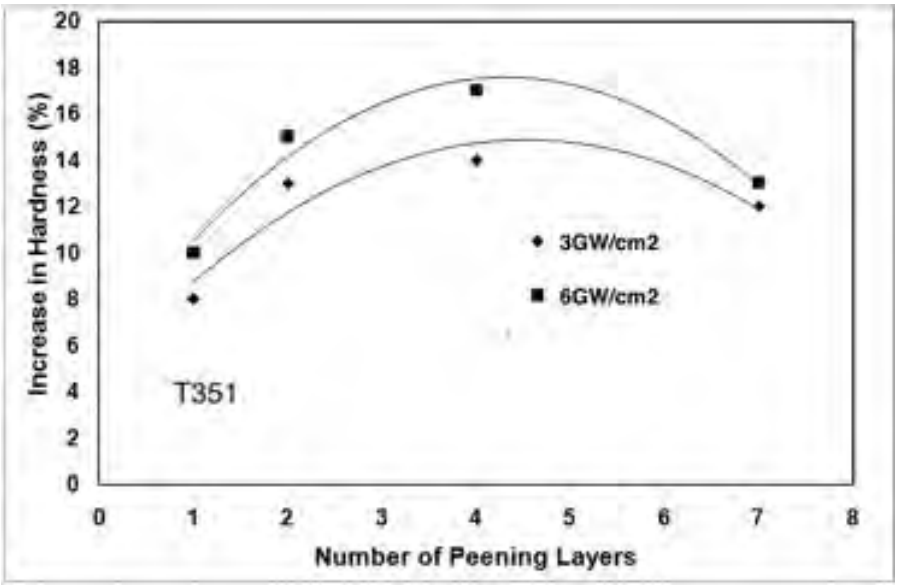

Figure 3.17: Effect of peen layers on hardness for the T351 condition

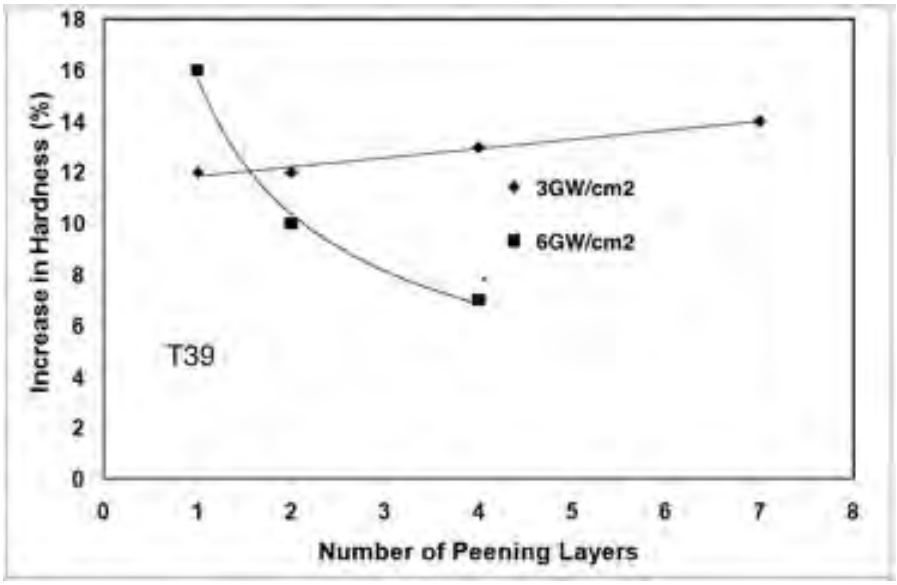

Figure 3.18: Effect of peen layers on hardness for the T39 condition

In terms of residual stress, figures 3.19 and 3.20 clearly show that whilst more layers can have a beneficial effect on the magnitude of compressive residual stress, increasing the power density too far (which in this case means to 6 GW/cm^2) causes reverse yielding and decreases the magnitude of the surface compressive residual stress. This is particularly noticeable for the T39 condition.

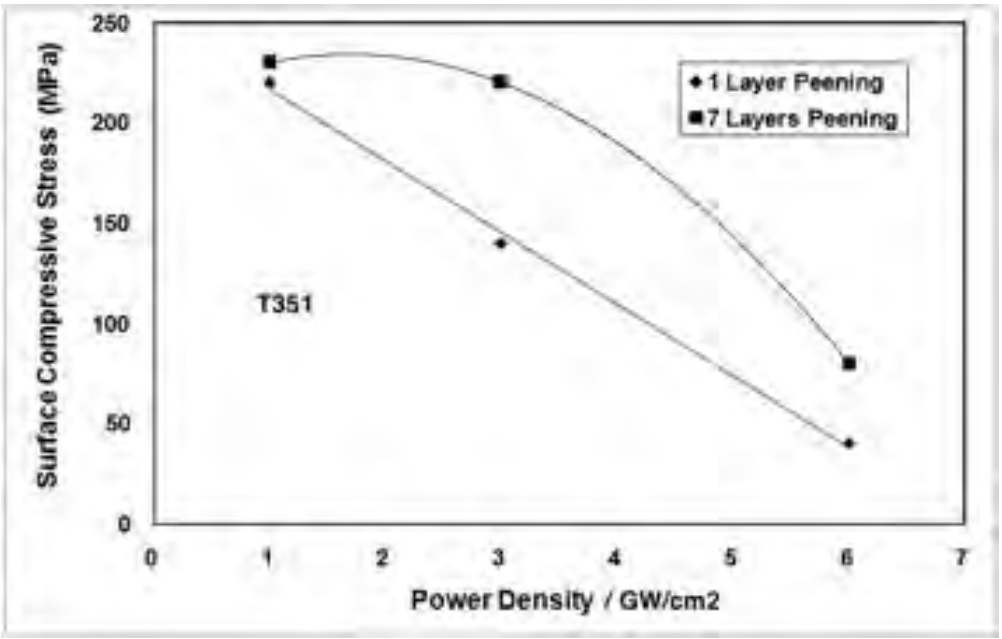

Figure 3.19: Effect of power density and number of peen layers on surface residual stress for the T351 condition

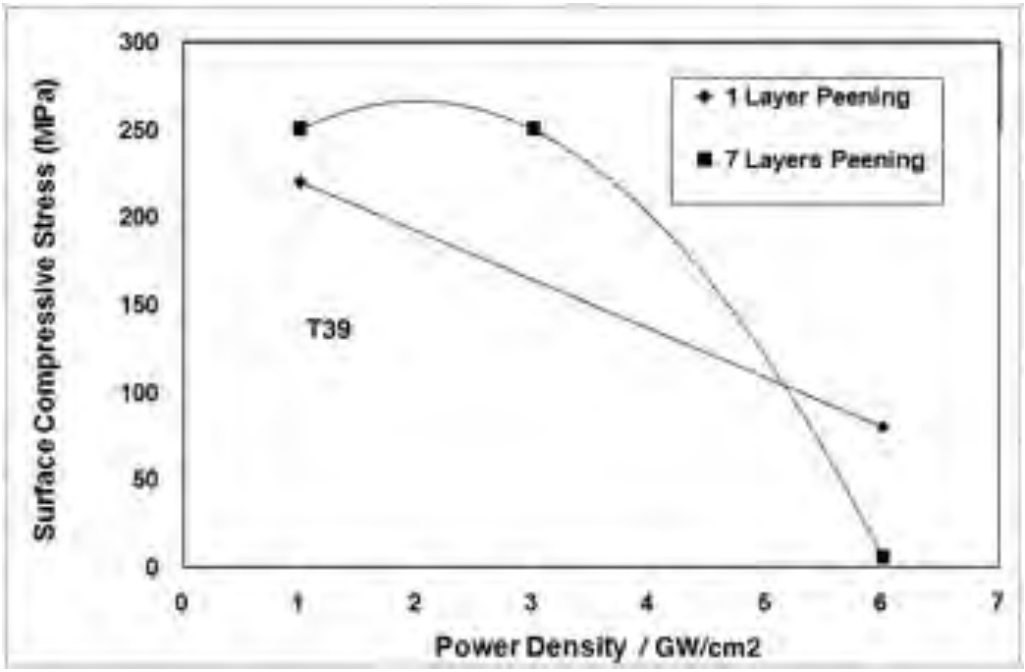

Figure 3.20: Effect of power density and number of peen layers on surface residual stress for the T39 condition

Chapter 4. Results and discussion from textured Al-2099

4.1 Hardness

The specimen was polished for Vickers measurement with a load of 5 kgF. Figure 4-1b shows the Vickers microhardness map for the Al-2099 extruded T bar. The result shows a higher hardness (HV5 140) in the flange section. A through-thickness hardness variation can also observed in the hardness map. The through-thickness hardness variation may reflect different textures in the material.

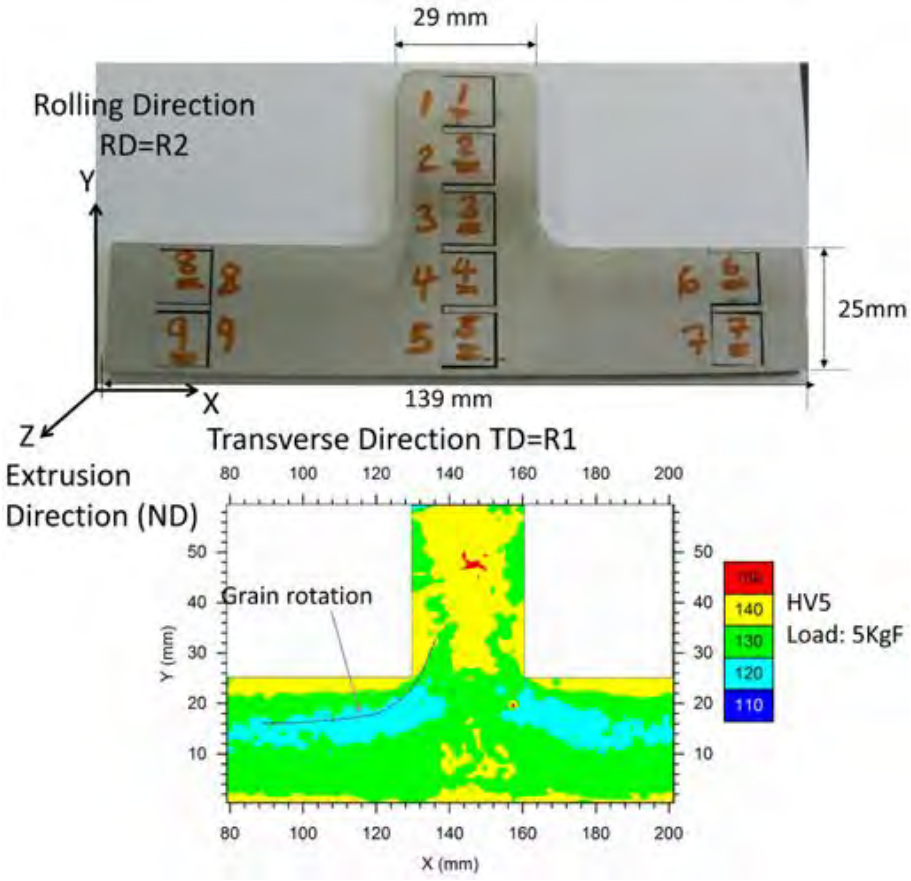

Figure 4-1: (a) Specimen Geometry of the extruded bar showing the axis definition (b) corresponding Vickers microhardness map.

4.2 Texture

Preferred crystallographic orientation or texture results in anisotropic mechanical properties in polycrystalline material. Al-Li extrusion products show in-plane and through-thickness texture variation; and a texture difference in the web and flange section of extruded bar (Hales, Hafley 1998).

Figure 4-2 presents the reconstructed (111), (200) and (220) pole figures for specimens 1-7. Specimens 1, 2 and 3 show typical <111> fibre texture. The results are consistent with the literature (Denzer et al. 1992, Jata, Singh 2014). The flange section has a rolling-type texture.

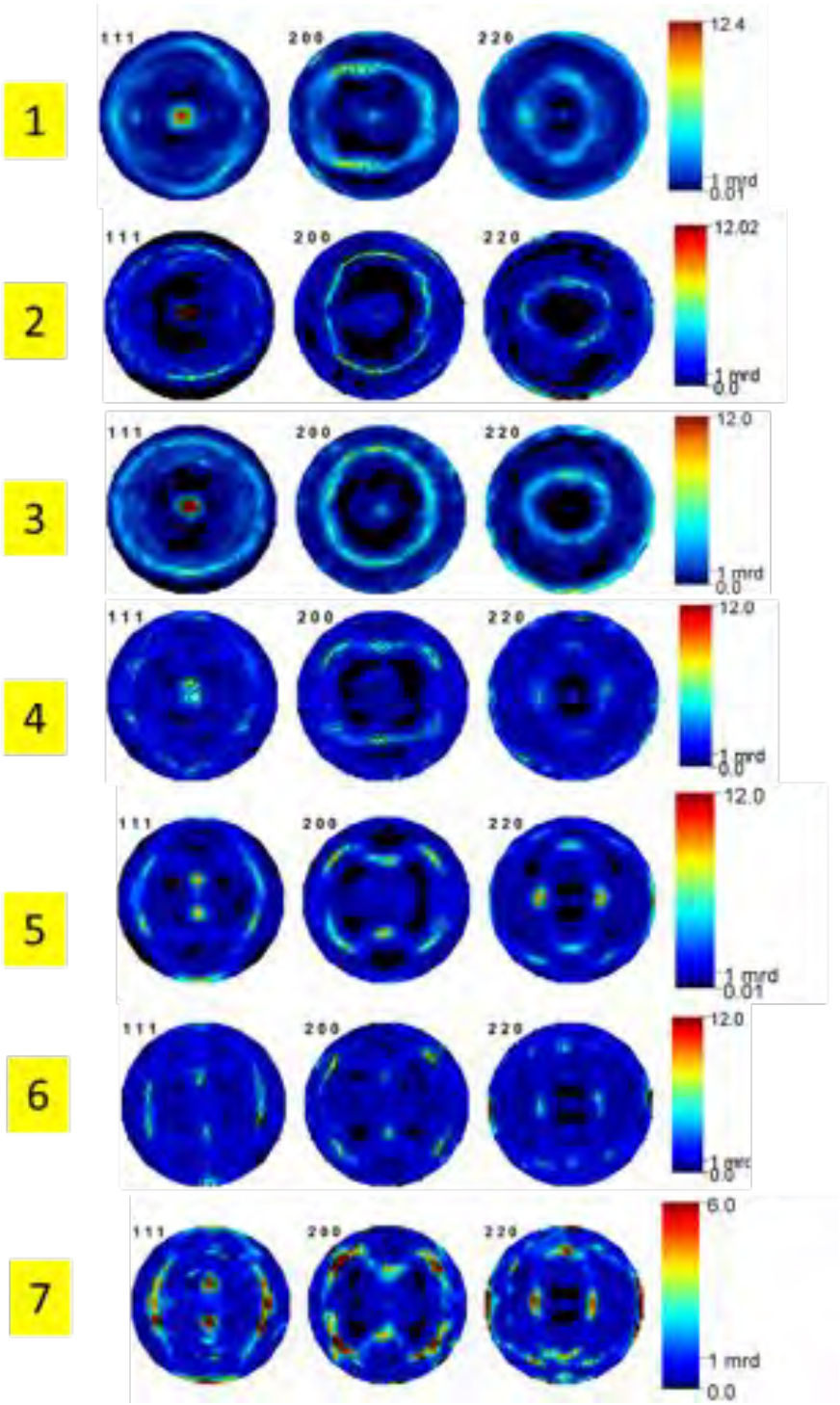

Figure 4-2: (111), (200), and (220) pole figures for specimens 1 to 7 as shown in Figure 2-10 b.

4.3 Residual Stress

Residual stresses in extruded Al-2099 specimens owing to single spot peening on XY, YZ, and ZX planes were measured using incremental hole drilling. Specimens from both web and flange sections were characterised and compared.

4.3.1 Effect of texture on residual stress generation

Figure 4-3a compares the residual stress distribution between ZY, XY and ZX orientations (specimen 1, 2, 3) extracted from the centre flange section of the specimen with fibre texture; and Figure 4-3c shows that for specimens 4, 5, and 6 which were extracted from the web section with rolling texture. Refer to figure 4-1 for the locations from which the samples were extracted.

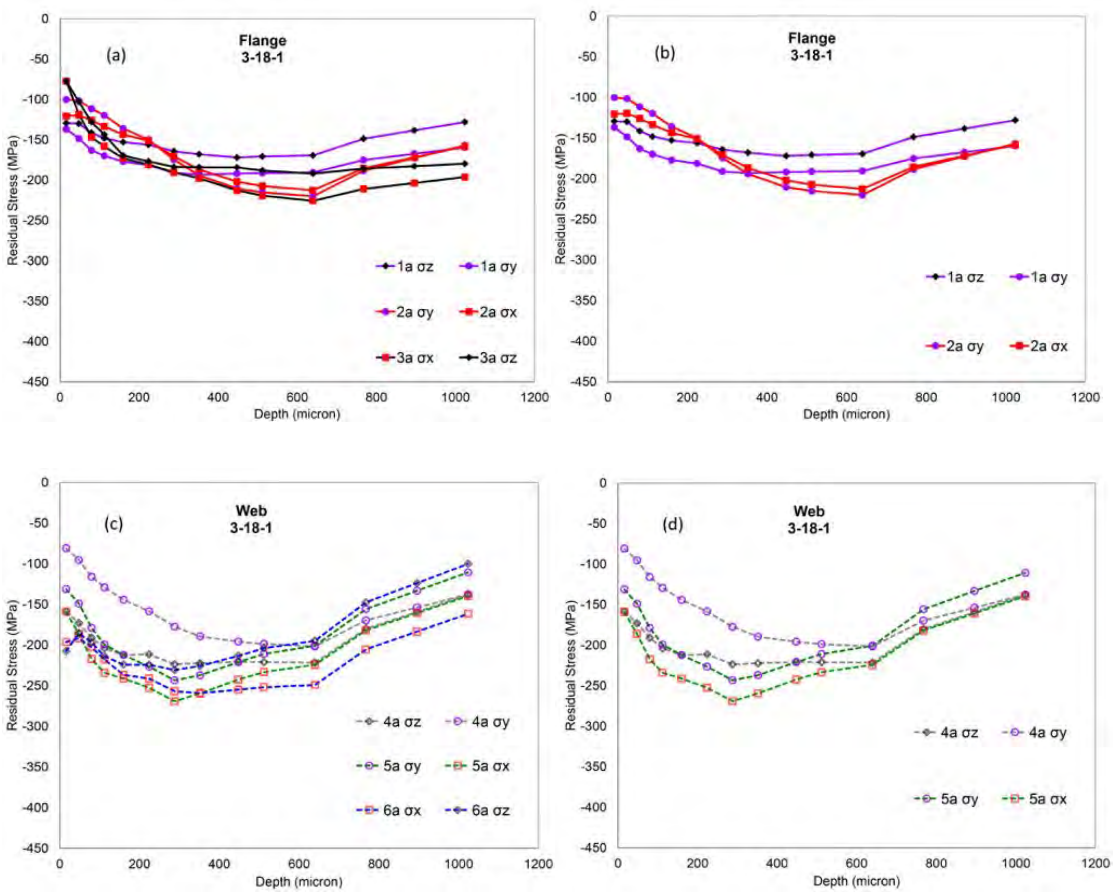

Figure 4-3: Comparison of residual stress profiles between samples extracted from the web: (a) and (b), and the centre: (c) and (d) after laser shock peening at 3-18-1 (GW/cm2-ns-layer) on the XY (samples 2 and 5), ZY (samples 1 and 4) and ZX (samples 3 and 6) planes of the specimens. Refer to figure 4-1 for the locations from which the samples were extracted.

After a single laser shot at 3 GW/cm² for 18 ns (3-18-1) the residual stress at the near surface of the specimens extracted from the flange (1a-3a) lies in the range of –100 to –150 MPa as shown in Figure 4-3a; whereas that for the specimens extracted from the web section (4a-6a) lies within –152 to –200 MPa, Figure 4-3c, after 1 shot. There is no significant variation in residual stresses observed between the XY, YZ, and ZX orientations in either flange specimens (1a-3a) or web specimens (4a-6a). Residual stresses were also measured in flange and web specimens peened with the same energy in 3 layers, Figure 4-4. In comparison to 1 layer, a difference is observed in the residual stress profiles between the orientations.

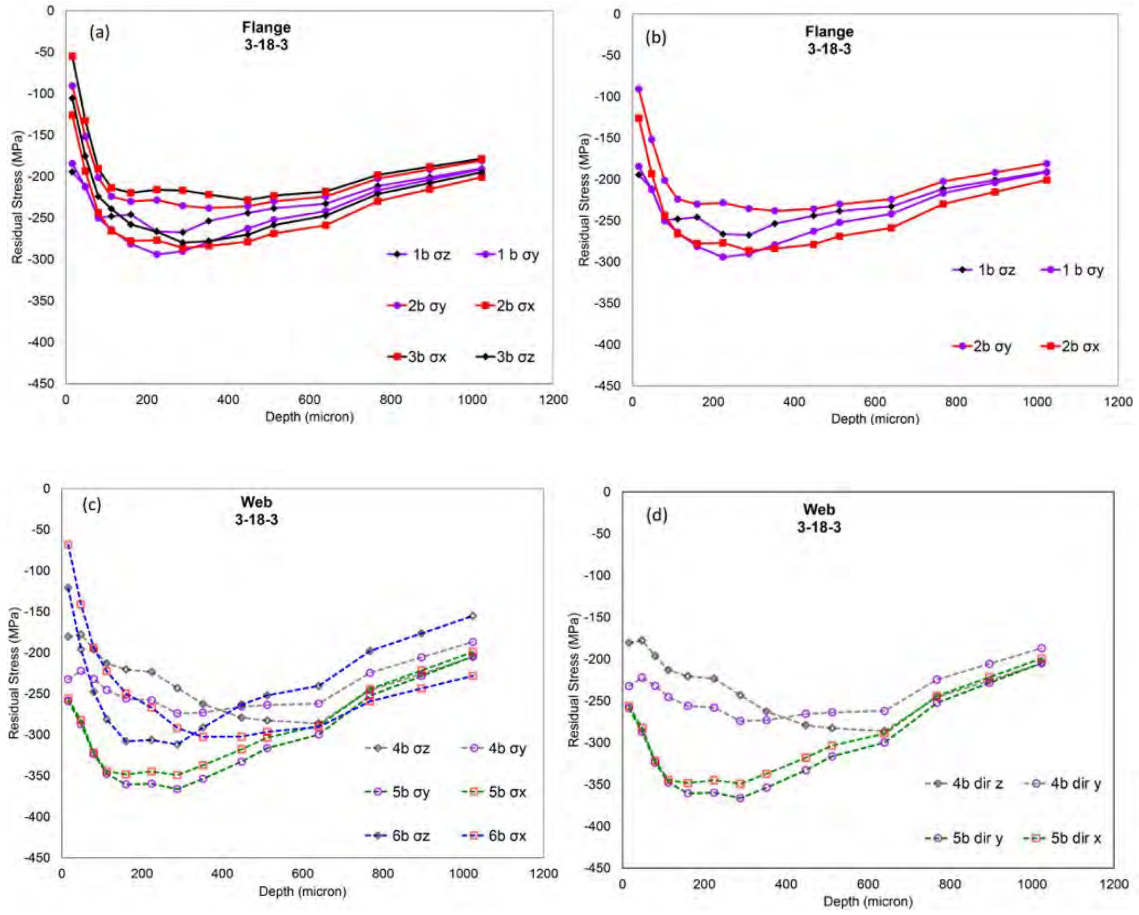

Figure 4-4: Residual stress distributions measured by incremental hole drilling technique shows the effect of texture (Flange vs. web of extruded T bar) for single shot peened specimens with conditions 3-18-1 (GW/cm²-ns-layer)

The highest surface stress as well as maximum compressive residual stress is evident in the XY orientation. In this orientation, the specimen was peened on the XY plane so that the normal direction to the peen spot lies along the longitudinal direction (Z).

Since a very weak texture is observed in the flange section little difference in the residual stress was observed between the YZ and ZX plane.

4.3.2 Effect of number of layers

Figure 4-5 shows the effect of the number of peening layers on the residual stress distribution in the XY orientation for (a) fibre texture specimen no. 2 and (b) rolling texture specimen no. 5. The maximum value of compression after 3 laser shots reached –275 MPa at a depth of ~300 μm.

Greater compression was observed in specimen 5 compared to specimen 2 after 1 hit and 3 hits. The surface residual stresses after 1 layer and 3 layers are –140 and –255 MPa respectively; and the maximum compressive residual stresses after 1 layer and 3 layers are –250 and –375 MPa respectively. The values of the compressive residual stresses are greatly increased with increasing number of layers, however, the overall shape of the residual stresses profiles are similar for specimen 5a and 5b. The possible reasons of higher residual stresses in the web specimens are as already explained.

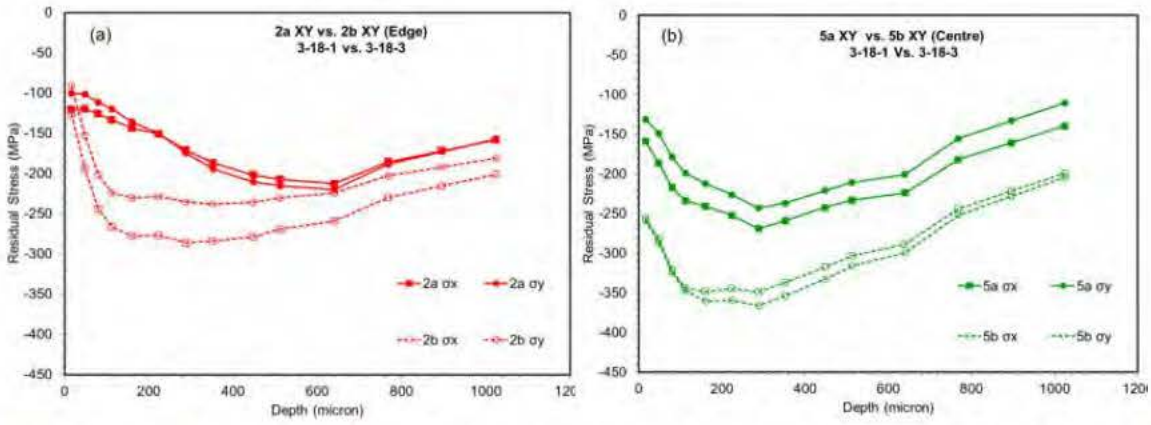

Figure 4-5: Effect of number of layers on the residual stress profiles in (a) flange (specimen 2a and 2b) and (b) web (specimen 5a and 5b) specimens.

4.4 Conclusions

1. Extruded Al-2099 T-bar has a strong <111> fibre texture in the centre T-section and weak rolling texture in the edge section.
2. The texture in the material has a noticeable effect on the residual stress generation in that different residual stress profiles are obtained from peening onto samples extracted from different sections of the extrusion. This has the implication that a

laser peen treatment will produce different profiles of residual stress when applied in the different areas of such a product form.

3. Laser peening on the XY plane resulted in higher surface and subsurface compressive residual stress compared to other two orientations after 3 layers. Equi-biaxial residual stresses are induced in the web section whereas a slightly bi-axial residual stresses is found in the flange section after peening at 3-18-3.
4. The maximum compressive residual stress values are increased by 70% and 65% for the web and the flange respectively after 3 hits.

Summary

This study has examined how the response of a material to laser peening is dependent on its cyclic plasticity behaviour and crystallographic texture. These factors are influenced by heat treatment and by thermomechanical processing.

We have demonstrated that there are differences in responses owing to changes in yield stress and hardening exponents. A material in a relatively soft condition with high work hardening capacity will show increasing surface compressive residual stress with repeated peen layers; but a harder condition of the same alloy shows less difference from repeat peening and may in fact show impaired results at higher levels of peen power density.

This result demonstrates the need to characterise the peen response of materials in the actual heat treatment conditions in which that they will be used.

The second part of the study looked at the response of an alloy with different textures. The results show that different residual stress profiles are obtained when peening onto different regions of an extrusion that has different textures. Some differences in hardness were seen across the section, and this will also have affected the residual stresses as determined in the first part of the study: the interaction between the two mechanisms will merit further investigation.

A key finding from this part of the study is that different residual stress profiles can be obtained when peening onto a single component with a non-simple geometry. This is particularly important as many modelling procedures, whether they are physics-based such as finite-element modelling or semi-empirical such as the eigenstrain approach, effectively assume that the material is a continuum and the same response will be obtained at all locations.

Acknowledgements

Effort sponsored by the Air Force Office of Scientific Research, Air Force Material Command, USAF, under grant number FA8655-12-1-2084. The U.S. Government is authorized to reproduce and distribute reprints for Government purpose notwithstanding any copyright notation thereon. The views and conclusions contained herein are those of the authors and should not be interpreted as necessarily representing the official policies or endorsements, either expressed or implied, of the Air Force Office of Scientific Research or the U.S. Government. The authors would like to thank Dr Markus Heinimann at Alcoa Inc. for the provision of the material studied in the project. Thanks are also due to Dr Andy Fitch at ESRF, Grenoble, France; Dr Winfried Kockelmann, ISIS, UK; Mr Pete Ledgard and Mr Stan Hiller at The Open University, and Dr Philip Whitehead at Stresscraft, UK for technical support. MEF is grateful for funding from the Lloyd's Register Foundation, a charitable foundation helping to protect life and property by supporting engineering-related education, public engagement and the application of research.

References

Altenberger, I., Nalla, R.K., Noster, U., Scholtes, B. & Ritchie, R.O. 2002, "On the fatigue behaviour and associated effect of residual stresses in deep-rolled and laser shock peened Ti-6Al-4V alloys at ambient and elevated temperatures", *7th Natl Turbine Engine High Cycle Fatigue Confrence*, May 2002.

Beegan, D., Chowdhury, S. & Laugier, M.T. 2003, "A nanoindentation study of copper films on oxidised silicon substrates", *Surface and Coatings Technology*, vol. 176, no. 1, pp. 124-130.

Clauer, A. 1996, *Laser shock peening for fatigue resistance: Surface performance of titanium.* , PA, USA.

Clauer, A.H., Walters, C.T. & and Ford, S.C. 1983, *The Effects of Laser Shock Processing on the Fatigue Properties of 2024-T3 Aluminum*, American Society for Metals, Metals Park, Ohio.

Denzer, D.K., Hollinshead, P.A., Liu, J., Armanie, K.P. & Rioja, R.J. 1992, "Texture and Properties of 2090, 8090 and 7050 Extruded Products, Ibid. (II) (1992), pp.903.", *VI International Aluminium-Lithium Conference*, vol. ii, pp. 903-909.

Dorman, M., Toparli, M.B., Smyth, N., Cini, A., Fitzpatrick, M.E. & Irving, P.E. 2012, "Effect of laser shock peening on residual stress and fatigue life of clad 2024 aluminium sheet containing scribe defects", *Materials Science and Engineering: A*, vol. 548, no. 0, pp. 142-151.

Fairand, B.P., Wilcox, B.A., Gallagher, W.J. & and Williams, D.N. 1972, "Laser shock induced microstructural and mechanical property changes in 7075 aluminum", *Journal of Applied Physics*, vol. 43(9), pp. 3893-3895.

Giummarra, C., Thomas, B. & Rioja, R.J. 2007, "New aluminum lithium alloys for aerospace applications. In *Proceedings of the light metals technology conference*.", *light metals technology*, .

Grant, P.V., Lord, J.D. & Whitehead, P. 2006, *The Measurement of Residual Stresses by the Incremental Hole Drilling Technique - Issue 2*, The National Physical Laboratory (NPL).

Hales, S.J. & Hafley, R.A. 1998, "Texture and anisotropy in Al-Li alloy 2195 plate and near-net-shape extrusions", *Materials Science and Engineering: A*, vol. 257, no. 1, pp. 153-164.

Hatamleh, O., Lyons, J. & Forman, R. 2007, "Laser and shot peening effects on fatigue crack growth in friction stir welded 7075-T7351 aluminum alloy joints", *International Journal of Fatigue*, vol. 29, no. 3, pp. 421-434.

Hill, M.R., Pistochini, T.E. & and Dewald, A.T. 2005, "Optimisation of residual stress and fatigue life in laser peened components.", *9th International Conference on Shot Peening (ICSP-9), Paris, France.*, ed. A. Niku-Lari, IITTInternational, Paris: 156-162., , pp. 156.

Hong, Z. & and Chengye, Y. 1998, "Laser shock processing of 2024-T62 aluminum alloy.", *Materials Science and Engineering A*, vol. 257(2), pp. 322-327.

Jata, K.V., Panchanadeeswaran, S. & Vasudevan, A.K. 1998, "Evolution of texture, micro structure and mechanical property anisotropy in an Al-Li-Cu alloy", *Materials Science and Engineering: A*, vol. 257, no. 1, pp. 37-46.

Jata, K.V. & Singh, A.K. 2014, "Chapter 5 - Texture and Its Effects on Properties in Aluminum–Lithium Alloys" in *Aluminum-lithium Alloys*, eds. N.E. Prasad, A.A. Gokhale & R.J.H. Wanhill, Butterworth-Heinemann, Boston, pp. 139-163.

Kese, K. & Li, Z.C. 2006, "Semi-ellipse method for accounting for the pile-up contact area during nanoindentation with the Berkovich indenter", *Scripta Materialia*, vol. 55, no. 8, pp. 699-702.

Khan, M.K., Fitzpatrick, M.E., Hainsworth, S.V., Evans, A.D. & Edwards, L. 2011, "Application of synchrotron X-ray diffraction and nanoindentation for the determination of residual stress fields around scratches", *Acta Materialia*, vol. 59, no. 20, pp. 7508-7520.

King, A., Steuwer, A., Woodward, C. & Withers, P.J. 2006, "Effects of fatigue and fretting on residual stresses introduced by laser shock peening", *Materials Science and Engineering: A*, vol. 435-436, pp. 12-18.

Kockelmann, W., Chapon, L.C. & Radaelli, P.G. 2006, "Neutron texture analysis on GEM at ISIS", *Physica B: Condensed Matter*, vol. 385–386, Part 1, no. 0, pp. 639-643.

Liu, Q., Yang, C.H., Ding, K., Barter, S.A. & Ye, L. 2007, "The effect of laser power density on the fatigue life of laser-shock-peened 7050 aluminium alloy", *Fatigue & Fracture of Engineering Materials & Structures*, vol. 30, no. 11, pp. 1110-1124.

Lutterotti, L., Matthies, S., Wenk, H.-., Schultz, A.S. & Richardson, J.W. 1997, "Combined texture and structure analysis of deformed limestone from time-of-flight neutron diffraction spectra", *Journal of Applied Physics*, vol. 81, no. 2, pp. 594-600.

Montross, C.S., Wei, T., Ye, L., Clark, G. & Mai, Y. 2002, "Laser shock processing and its effects on microstructure and properties of metal alloys: a review", *International Journal of Fatigue*, vol. 24, no. 10, pp. 1021-1036.

Newey, D., Wilkins, M.A. & Pollock, H.M. 1982, "An ultra-low-load penetration hardness tester", *Journal of Physics E: Scientific Instruments*, vol. 15, no. 1, pp. 119-122.

Nikitin, I., Scholtes, B., Maier, H.J. & Altenberger, I. 2004, "High temperature fatigue behavior and residual stress stability of laser-shock peened and deep rolled austenitic steel AISI 304", *Scripta Materialia*, vol. 50, no. 10, pp. 1345-1350.

Oliver, W.C. & Pharr, G.M. 1992, "An improved technique for determining hardness and elastic modulus using load and displacement sensing indentation experiments", *Journal of Materials Research*, vol. 7, no. 06, pp. 1564-1583.

Pethica, J.B. 1982, "Microhardness tests with penetration depths less than ion implanted layer thickness" in *Ion Implantation Into Metals*, ed. V.A.G. PROCTER, Pergamon, , pp. 147-156.

Peyre, P. & Fabbro, R. 1995, "Laser shock processing: a review of the physics and applications", *Optical and Quantum Electronics*, vol. 27, no. 12, pp. 1213-1229.

Prime, M.B. 2001, "Cross-Sectional Mapping of Residual Stresses by Measuring the Surface Contour After a Cut", *Journal of Engineering Materials and Technology*, vol. 123, no. 2, pp. 162-168.

Rioja, R. & Liu, J. 2012, "The Evolution of Al-Li Base Products for Aerospace and Space Applications", *Metallurgical and Materials Transactions A*, vol. 43, no. 9, pp. 3325-3337.

Rodopoulos, C.A., Romero, J.S., Curtis, S.A., de, l.R. & Peyre, P. 2003, "Effect of controlled shot peening and laser shock peening on the fatigue performance of 2024-T351 aluminum alloy", *Journal of Materials Engineering and Performance*, vol. 12, no. 4, pp. 414-419.

Rubio-Gonz·lez, C., OcaÒa, J.L., Gomez-Rosas, G., Molpeceres, C., Paredes, M., Banderas, A., Porro, J. & Morales, M. 2004, "Effect of laser shock processing on fatigue crack growth and fracture toughness of 6061-T6 aluminum alloy", *Materials Science and Engineering A*, vol. 386, no. 1-2, pp. 291-295.

Ruschau, J.J., John, R., Thompson, S.R. & Nicholas, T. 1999, "Fatigue crack nucleation and growth rate behavior of laser shock peened titanium", *International Journal of Fatigue*, vol. 21, no. Supplement 1, pp. 199-209.

Saklakoglu, N., Gencalp Irizalp, S., Akman, E. & Demir, A. 2014, "Near surface modification of aluminum alloy induced by laser shock processing", *Optics and Laser Technology*, vol. 64, pp. 235-241.

Sathyajith, S., Kalainathan, S. & Swaroop, S. 2013, "Laser peening without coating on aluminum alloy Al-6061-T6 using low energy Nd:YAG laser", *Optics and Laser Technology*, vol. 45, no. 1, pp. 389-394.

Sticchi, M., Schnubel, D., Kashaev, N. & Huber, N. 2014, "Review of Residual Stress Modification Techniques for Extending the Fatigue Life of Metallic Aircraft Components", *Applied Mechanics Reviews*, vol. 67, no. 1, pp. 010801-010801.

Stone, D., LaFontaine, W.R., Alexopoulos, P., Wu, T.-. & Li, C. 1988, "An investigation of hardness and adhesion of sputter-deposited aluminum on silicon by utilizing a continuous indentation test", *Journal of Materials Research*, vol. 3, no. 01, pp. 141-147.

Suresh, S. & Giannakopoulos, A.E. 1998, "A new method for estimating residual stresses by instrumented sharp indentation", *Acta Materialia*, vol. 46, no. 16, pp. 5755-5767.

Tan, Y., Wu, G., Yang, J.M. & Pan, T. 2004, "Laser shock peening on fatigue crack growth behaviour of aluminium alloy", *Fatigue & Fracture of Engineering Materials & Structures*, vol. 27, no. 8, pp. 649-656.

Toparli, M.B. & Fitzpatrick, M.E. 2013, " Through Thickness Residual Stress Measurements by Neutron Diffraction and Hole Drilling in a Single Laser-Peened Spot on a Thin Aluminium Plate", *Materials Science Forum*, vol. 772, pp. 167-172.

Tuck, J.R., Korsunsky, A.M., Bull, S.J. & Davidson, R.I. 2001, "On the application of the work-of-indentation approach to depth-sensing indentation experiments in coated systems", *Surface and Coatings Technology*, vol. 137, no. 2–3, pp. 217-224.

Vasudevan, A.K., Fricke, W.G. & Panchanadeeswaran, S. 1988, "Synergistic effects of crystallographic texture and precipitation on the yield stress anisotropy in Al-Li-Cu-Zr alloy", *Proceedings of the 8th International Conference on Texture of Materials (ICOTOM-8)*, pp. 1071.

Wang, C., Zhou, L.C., Zhou, X., He, Q. & Li, W. 2010, "Experimental research on the effects of different overlapping rate in laser shock processing", *Proceedings of SPIE - The International Society for Optical Engineering*.

Wenk, H.-., Lutterotti, L. & Vogel, S.C. 2010, "Rietveld texture analysis from TOF neutron diffraction data", *Powder Diffraction*, vol. 25, no. 03, pp. 283-296.

Yang, J.M., Her, Y.C., Han, N. & Clauer, A. 2001, "Laser shock peening on fatigue behavior of 2024-T3 Al alloy with fastener holes and stopholes", *Materials Science and Engineering: A*, vol. 298, no. 1-2, pp. 296-299.

Zhang, X.Q., Li, H., Yu, X.L., Zhou, Y., Duan, S.W., Li, S.Z., Huang, Z.L. & Zuo, L.S. 2015, "Investigation on effect of laser shock processing on fatigue crack initiation and its growth in aluminum alloy plate", *Materials and Design*, vol. 65, pp. 425-431.

Zhang, Y.K., Lu, J.Z., Ren, X.D., Yao, H.B. & Yao, H.X. 2009, "Effect of laser shock processing on the mechanical properties and fatigue lives of the turbojet engine blades manufactured by LY2 aluminum alloy", *Materials & Design*, vol. 30, no. 5, pp. 1697-1703.

Zhang, Y., Zhang, S., Yu, C., Tang, Y., Zhang, H., Wu, H., Guo, D., Wang, S., Xia, X., Chen, M. & Dai, Y. 1997, "Laser shock-processing for fatigue and fracture resistance", *Science in China Series E: Technological Sciences*, vol. 40, no. 2, pp. 170-177.